TECHNICAL REPORT ARCCB-TR-93015

AUTOFRETTAGE --STRESS DISTRIBUTION UNDER LOAD AND RETAINED STRESSES AFTER DEPRESSURIZATION-- A MODIFIED PLANE-STRAIN CASE

BOAZ AVITZUR

APRIL 1993

US ARMY ARMAMENT RESEARCH,
DEVELOPMENT AND ENGINEERING CENTER
CLOSE COMBAT ARMAMENTS CENTER
BENÉT LABORATORIES
WATERVLIET, N.Y. 12189-4050

DISCLAIMER

The findings in this report are not to be construed as an official Department of the Army position unless so designated by other authorized documents.

The use of trade name(s) and/or manufacturer(s) does not constitute an official indorsement or approval.

DESTRUCTION NOTICE

For classified documents, follow the procedures in DoD 5200.22-M, Industrial Security Manual, Section II-19 or DoD 5200.1-R, Information Security Program Regulation, Chapter IX.

For unclassified, limited documents, destroy by any method that will prevent disclosure of contents or reconstruction of the document.

For unclassified, unlimited documents, destroy when the report is no longer needed. Do not return it to the originator.

REPORT DOCUMENTATION PAGE

Form Approved
OMB No. 0704-0188

1. AGENCY USE ONLY *(Leave blank)*

2. REPORT DATE
April 1993

3. REPORT TYPE AND DATES COVERED
Final

4. TITLE AND SUBTITLE
AUTOFRETTAGE--STRESS DISTRIBUTION UNDER LOAD AND RETAINED STRESSES AFTER DEPRESSURIZATION--A MODIFIED PLANE-STRAIN CASE

5. FUNDING NUMBERS
AMCMS: 6126.24.H180.0
PRON: M721F221M7

6. AUTHOR(S)
Boaz Avitzur

7. PERFORMING ORGANIZATION NAME(S) AND ADDRESS(ES)
U.S. Army ARDEC
Benet Laboratories, SMCAR-CCB-TL
Watervliet, NY 12189-4050

8. PERFORMING ORGANIZATION REPORT NUMBER
ARCCB-TR-93015

9. SPONSORING / MONITORING AGENCY NAME(S) AND ADDRESS(ES)
U.S. Army ARDEC
Close Combat Armaments Center
Picatinny Arsenal, NJ 07806-5000

10. SPONSORING / MONITORING AGENCY REPORT NUMBER

11. SUPPLEMENTARY NOTES
Accepted for presentation at the Army Symposium on Solid Mechanics, Plymouth, MA, 17-19 August 1993.

12a. DISTRIBUTION / AVAILABILITY STATEMENT
Approved for public release; distribution unlimited

12b. DISTRIBUTION CODE

13. ABSTRACT *(Maximum 200 words)*
There is a long-standing interest in developing a capability to predict the distribution of retained stresses in thick-walled pressure vessels after the removal of an internal pressure--post autofrettage. The key to such a prediction is in the capacity to compute the stress distribution in a vessel while under externally imposed stress sufficient enough to cause at least partial plastic deformation. A good approximation of the stress distribution was developed by Mises in his 1913 plane-stress solution. The fact that such vessels are not representative of the plane-stress condition not withstanding, Mises recognized that his solution was mathematically restricted to a limited range of vessels' wall ratios. More recently, Avitzur offered a solution similar to that of Mises, but for a plane-strain condition. Depending on the material's Poisson's factor, Avitzur's solution is also mathematically applicable for a limited range of vessels' wall ratios only. The wall ratio, beyond which Avitzur's solution in plane-strain is not applicable, is a few times larger than that which limits Mises' solution in plane-stress. This work introduces a modification to Avitzur's solution in plane-strain, which makes its applicability unlimited.

14. SUBJECT TERMS
Autofrettage, Thick-Walled Tubes, Stress Distribution, Retained Stress, Tresca's Yield Criterion, Mises' Yield Criterion, Plane-Stress, Plane-Strain

15. NUMBER OF PAGES
63

16. PRICE CODE

17. SECURITY CLASSIFICATION OF REPORT	18. SECURITY CLASSIFICATION OF THIS PAGE	19. SECURITY CLASSIFICATION OF ABSTRACT	20. LIMITATION OF ABSTRACT
UNCLASSIFIED	UNCLASSIFIED	UNCLASSIFIED	UL

TABLE OF CONTENTS

List of Illustrations

NOMENCLATURE

a	≡	tube's bore radius
b	≡	tube's outer radius
E	≡	material's modulus of elasticity
p	≡	pressure
p_i	≡	internal pressure at the tube's bore
p_o	≡	external pressure at the tube's outer diameter
r	≡	radial distance
z	≡	coordinate's direction in a Cartesian and/or cylindrical coordinate systems
δ	≡	$1 - v + v^2$
ϵ	≡	strain
η	≡	$(1-2v)^2$
v	≡	Poisson's factor
v_e	≡	material's (elastically determined) Poisson's factor
$v_{(r)}$	≡	an equivalent Poisson's factor at radius r in the plastic region, $a \leq r \leq \rho$
σ	≡	stress
σ_o	≡	material's yield strength
ρ	≡	radius of elastic-plastic interface

<u>Subscripts</u>

i	≡	at the tube's inner diameter
o	≡	at the tube's outer diameter
r	≡	a coordinate's plane and/or a coordinate's direction in a cylindrical coordinate system
z	≡	a coordinate's plane and/or a coordinate's direction in a cylindrical and/or in Cartesian coordinate systems
θ	≡	a coordinate's plane and/or a coordinate's direction in a cylindrical coordinate system
( )	≡	a subscript inside parentheses indicates a specific geometrical location, i.e., $\sigma_{rr(a)} = \sigma_{rr}$ @ $r = a$ or $\sigma_{\theta\theta(\rho)} = \sigma_{\theta\theta}$ @ $r = \rho$

INTRODUCTION

A process whereby thick-walled pressure vessels are pressurized beyond their elastic limit has long been recognized as beneficial to increase the service life of the vessels, particularly when subjected to repeated loading and unloading. This process, known as autofrettage, drew the attention of Mises (ref 1), who, in 1913, offered a mathematical equation correlating the stress distribution within the vessel's wall with the pressure at the vessel's interior. Mises' solution in plane-stress assumes that the stress distribution in the elastic region, $\rho \leq r \leq b$, of an autofrettaged tube is the same as that of an elastically stressed tube of the same dimensions (namely of the same outer diameter (OD) and whose inner diameter (ID) $= \rho$) subjected to an internal pressure, $p_i = -\sigma_{rr(\rho)}$, for which plastic deformation will commence at its inner surface, $r_i = \rho$ (ref 2). The inner layer, $a \leq r \leq \rho$, undergoes plastic deformation and its state of stress, including the elastic-plastic interface, can not exceed

$$\tfrac{1}{2}\left[(\sigma_{11}-\sigma_{22})^2 + (\sigma_{22}-\sigma_{33})^2 + (\sigma_{33}-\sigma_{11})^2\right] = \sigma_0^2 \tag{1}$$

where σ_{ii} are the principal components of the stress and σ_o is the material's yield strength in uniaxial loading. Equation (1) is a special case of Mises' yield criterion.

According to Lamé's equations (ref 3), the stress distribution in an elastically pressurized thick-walled vessel is

$$\sigma_{rr(r)} = -\frac{\left(\frac{b}{r}\right)^2 - 1}{\left(\frac{b}{a}\right)^2 - 1} p_i$$

and (2)

$$\sigma_{\theta\theta(r)} = \frac{\left(\frac{b}{r}\right)^2 + 1}{\left(\frac{b}{a}\right)^2 - 1} p_i$$

where $p_i \equiv$ internal hydrostatic pressure (at the vessel's bore). Thus, at the elastic-plastic interface where $\sigma_{rr(\rho)}$ replaces $-p_i$ (in Eq. (2)), for Mises' yield criterion to prevail at $r = \rho$ in plane-stress

$$\sigma_{rr(\rho)} = -\frac{\left(\frac{b}{\rho}\right)^2 - 1}{\sqrt{3\left(\frac{b}{\rho}\right)^4 + 1}} \cdot \sigma_o \tag{3a}$$

and

$$\sigma_{\theta\theta(\rho)} = \frac{\left(\frac{b}{\rho}\right)^2 + 1}{\sqrt{3\left(\frac{b}{\rho}\right)^4 + 1}} \cdot \sigma_o \tag{3b}$$

Thus, by replacing $-\sigma_{rr(\rho)}$ for p_i in Eq. (2), one gets the stress distribution in the elastic region, $\rho \le r \le b$

$$\sigma_{rr(r)} = -\frac{\left(\frac{b}{r}\right)^2 - 1}{\sqrt{3\left(\frac{b}{\rho}\right)^4 + 1}} \cdot \sigma_o \tag{4a}$$

and

$$\sigma_{\theta\theta(r)} = \frac{\left(\frac{b}{r}\right)^2 + 1}{\sqrt{3\left(\frac{b}{\rho}\right)^4 + 1}} \cdot \sigma_o \tag{4b}$$

It can be shown (ref 4) that for equilibrium to prevail in the r-θ plane

$$\frac{d\sigma_{rr}}{\sigma_{\theta\theta} - \sigma_{rr}} = \frac{dr}{r} \tag{5}$$

Lamé's equations (Eq. (2) in this report or in their more comprehensive form (ref 2)) satisfy the condition for equilibrium. Hence, equilibrium prevails in the entire elastic region, $\rho \le r \le b$, as described by Eq. (2) or Eqs. (4a) and 4(b). However, for the plastically deformed region, $a \le r \le \rho$, Mises applied his yielding criterion (Eq. (1)) to Eq. (5) and used Eq. (3b) as the boundary condition at $r = \rho$, thus arriving at the following

$$\ln\frac{r}{\rho} = -\,¼\left\{\ln\frac{\left[\sqrt{3}\cdot\sqrt{\frac{4}{3}\left(\frac{\sigma_o}{\sigma_{rr(r)}}\right)^2 - 1} + 1\right]^2}{4\left(\frac{\sigma_o}{\sigma_{rr(r)}}\right)^2} - \ln\frac{4\left(\frac{b}{\rho}\right)^4}{3\left(\frac{b}{\rho}\right)^4 - 1}\right.$$

$$\left.-2\cdot\sqrt{3}\left[\tan^{-1}\sqrt{\frac{4}{3}\left(\frac{\sigma_o}{\sigma_{rr(r)}}\right)^2 - 1} - \tan^{-1}\frac{3\left(\frac{b}{\rho}\right)^2 + 1}{\sqrt{3}\left[\left(\frac{b}{\rho}\right)^2 - 1\right]}\right]\right\} \tag{6}$$

However, Mises recognized that Eq. (6) is solvable only in the range

$$-\frac{2}{\sqrt{3}}\,\sigma_o \le \sigma_{rr(r)} \le \frac{2}{\sqrt{3}}\,\sigma_o$$

Depending on the wall ratio of the elastic region, b/ρ, this sets the following equation, Eq. (7), as the limiting wall ratio, ρ/a, of the plastic region for which Mises' solution, Eq. (6), is applicable

$$\ln\frac{\rho}{a} \le ¼\left\{\ln ⅓ - \ln\frac{4\left(\frac{b}{\rho}\right)^4}{3\left(\frac{b}{\rho}\right)^4 + 1} + 2\sqrt{3}\cdot\tan^{-1}\frac{3\left(\frac{b}{\rho}\right)^2 + 1}{\sqrt{3}\left[\left(\frac{b}{\rho}\right)^2 - 1\right]}\right\} \tag{7}$$

Solving Eq. (7) for the case of 100 percent autofrettage ($\rho = b$), Mises concluded that his solution is limited to vessels of wall ratio $b/a \le 2.9615$ (or conversely, $a/b \ge 0.3376665$).

TRESCA'S YIELD CRITERION

Assuming that Tresca's yield criterion, $\sigma_{11} - \sigma_{22} = \sigma_o$, prevails (ref 5) in the plastic region, the equation of equilibrium (Eq. (5)) is simplified and becomes

$$\frac{dr}{r} = \frac{d\sigma_{rr}}{\sigma_o} \tag{8}$$

where σ_o is a constant. Hence, its solution is simplified (compared to Eq. (6)), and it becomes

$$\ln\frac{r}{\rho} = \frac{1}{\sigma_o}\cdot\left\{\sigma_{rr(r)} - \sigma_{rr(\rho)}\right\} \tag{9}$$

The radial stress, $\sigma_{rr(\rho)}$, at the elastic-plastic interface, satisfying both Tresca's yield criterion and Lamé's solution simultaneously, is computed as

$$\sigma_{rr(\rho)} = -\frac{\left(\frac{b}{\rho}\right)^2 - 1}{2\left(\frac{b}{\rho}\right)^2} \cdot \sigma_o \tag{10}$$

MISES' YIELD CRITERION IN PLANE-STRAIN

Since plastic deformation assumes to preserve the material's volume, Hill (ref 6) suggested that "for large plastic deformation in plane-strain, the stress σ_{zz}, perpendicular to the plane of flow may be equal to the mean, $\frac{1}{2}(\sigma_{xx} + \sigma_{yy})$, of the other two normal stresses to a very good approximation *after a plastic strain of a few times the yield point strain*." Applying this relation (among the axial stress, σ_{zz}, the radial stress, σ_{rr}, and the tangential stress, $\sigma_{\theta\theta}$) to Mises' yield criterion, Eq. (1), results in

$$\sigma_{\theta\theta} - \sigma_{rr} = \frac{2}{\sqrt{3}}\sigma_o \tag{11}$$

which is equivalent to multiplying the yield strength in Tresca's solution by $2/\sqrt{3}$, thus enjoying all the mathematical simplifications associated with Tresca's yield criterion. Stacey and Webster (ref 7) and others capitalized on this mathematical convenience. However, Avitzur (ref 8) questioned the applicability of Hill's approximation of the axial stress, σ_{zz}, to the problem at hand on the following grounds:

1. The method by which Stacey and Webster (ref 7) apply this approximation increases all the stress components in the elastic region, $\rho \leq r \leq b$, by a factor of $2/\sqrt{3}$. This discrepancy is carried over to the 'after depressurization' condition.

2. The plastic strain encountered during autofrettage is rarely a "few times the yield point strain," and certainly not in the vicinity of the elastic-plastic interface, $r = \rho$.

Instead, Avitzur (ref 2) computed the principal stress components at the elastic-plastic interface and in plane-strain as

$$\sigma_{rr(\rho)} = -\frac{\left(\frac{b}{\rho}\right)^2 - 1}{\sqrt{3\left(\frac{b}{\rho}\right)^4 + (1-2\nu)^2}} \cdot \sigma_o \tag{12a}$$

$$\sigma_{\theta\theta(\rho)} = \frac{\left(\frac{b}{\rho}\right)^2 + 1}{\sqrt{3\left(\frac{b}{\rho}\right)^4 + (1-2\nu)^2}} \cdot \sigma_o \tag{12b}$$

$$\sigma_{zz(\rho)} = + \frac{2\nu}{\sqrt{3\left(\frac{b}{\rho}\right)^4 + (1-2\nu)^2}} \cdot \sigma_o \tag{12c}$$

Applying $p_i = -\sigma_{rr(\rho)}$ from Eq. (12a) to the Lamé equations (Eq. (2)) one gets

$$\sigma_{rr(r)} = - \frac{\left(\frac{b}{r}\right)^2 - 1}{\sqrt{3\left(\frac{b}{\rho}\right)^4 + (1-2\nu)^2}} \cdot \sigma_o \tag{13a}$$

$$\sigma_{\theta\theta(r)} = \frac{\left(\frac{b}{r}\right)^2 + 1}{\sqrt{3\left(\frac{b}{\rho}\right)^4 + (1-2\nu)^2}} \cdot \sigma_o \tag{13b}$$

$$\sigma_{zz(r)} = + \frac{2\nu}{\sqrt{3\left(\frac{b}{\rho}\right)^4 + (1-2\nu)^2}} \cdot \sigma_o \tag{13c}$$

for the stress distribution in the elastic region, $\rho \leq r \leq b$.

Assuming that in the plastic region, $a \leq r \leq \rho$, the elastic component of strain is dominating, Avitzur (ref 2) assumed that the same Hooke's Law for the relation between the three principal components of stress, σ_{rr}, $\sigma_{\theta\theta}$, and σ_{zz}, that prevail in the elastic region is being preserved throughout this region also. Applying Hooke's Law to Mises' yield criterion and consequently to the equation of equilibrium, and using Eq. (12a) as the boundary condition at $r = \rho$, Avitzur concluded that

$$\ln\frac{r}{\rho} = -\frac{1}{4}\left\{\ln\frac{\left[\sqrt{\frac{3}{\eta}}\cdot\sqrt{\frac{4\delta}{3\eta}\left(\frac{\sigma_o}{\sigma_{rr(r)}}\right)^2-1}+1\right]^2}{4\frac{\delta}{\eta^2}\left(\frac{\sigma_o}{\sigma_{rr(r)}}\right)^2} - \ln\frac{(3+\eta)\left(\frac{b}{\rho}\right)^4}{3\left(\frac{b}{\rho}\right)^4+\eta}\right.$$

$$\left. -2\sqrt{\frac{3}{\eta}}\cdot\left[\tan^{-1}\sqrt{\frac{4\delta}{3\eta}\left(\frac{\sigma_o}{\sigma_{rr(r)}}\right)^2-1} - \tan^{-1}\frac{3\left(\frac{b}{\rho}\right)^2+\eta}{\sqrt{3\eta}\left[\left(\frac{b}{\rho}\right)^2-1\right]}\right]\right\} \tag{14}$$

where $\delta = 1-v+v^2$, $\eta = (1-2v)^2 = 1-4v+4v^2$, and $3+\eta = 4\delta$. Equation (14) correlates the radial stress, $\sigma_{rr(r)}$, with its radial location, r. The tangential and axial components of the stress are derived thereof (see reference 2).

The derivation of Eq. (14), as well as of Mises' solution in plane-stress (Eq. (6) of this report)--together with the derivation of their equivalent equations for the respective cases when the external pressure, p_o, at the vessel's OD dominates the plastic deformation--are presented in Reference 9.

Like Mises' (ref 1) solution in plane-stress, Eq. (14) is limited to a radial stress in the range

$$-2\cdot\sqrt{\frac{\delta}{3\eta}}\cdot\sigma_o \le \sigma_{rr(r)} \le 2\cdot\sqrt{\frac{\delta}{3\eta}}\cdot\sigma_o$$

which imposes a wall ratio limitation of

$$\ln\frac{\rho}{a} \le \frac{1}{4}\left\{\ln\frac{\eta}{3} - \ln\frac{4\delta\left(\frac{b}{\rho}\right)^4}{3\left(\frac{b}{\rho}\right)^4+\eta} + 2\cdot\sqrt{\frac{3}{\eta}}\tan^{-1}\frac{3\left(\frac{b}{\rho}\right)^2+\eta}{\sqrt{3\eta}\left[\left(\frac{b}{\rho}\right)^2-1\right]}\right\} \tag{15}$$

Solving Eq. (15) for a fully plastically deformed thick-walled vessel, ρ = b, one gets b/a = 8.1619, or conversely, a/b = 0.1225, when the material's Poisson's factor is v = 0.25 and b/a = 14.4122, or conversely, a/b = 0.0694, when the material's Poisson's factor is v = 0.30 (compared to b/a = 2.9615 for Mises' plane-stress solution).

It can be shown (see Appendix A) that due to volume constancy in the plastic region, the ratio between the respective tangential strain at any given radius, r, versus the one at the material's yield point (at the elastic-plastic interface) is

$$\epsilon_{\theta\theta(r)}/\epsilon_{\theta\theta(\rho)} = \frac{\sqrt{1+(2+\epsilon_{\theta\theta(\rho)}) \cdot \epsilon_{\theta\theta(\rho)} \cdot \left(\frac{\rho}{r}\right)^2} - 1}{\epsilon_{\theta\theta(\rho)}} \tag{16}$$

Thus, for 100 percent autofrettage, when $\sigma_{rr(\rho)} = \sigma_{rr(b)} = 0$

$$\epsilon_{\theta\theta(\rho)} = \epsilon_{\theta\theta(b)} = 2\frac{1-\nu^2}{\sqrt{3+(1-2\nu)^2}} \cdot \frac{\sigma_o}{E}$$

(see Appendix B), and for a material having a yield strength of σ_o = 160,000 psi and modulus of elasticity, E = $30 \cdot 10^6$ psi, one gets (for the limiting cases of b/a = 8.1618 and b/a = 14.4122, respectively) $\epsilon_{\theta\theta(a)}/\epsilon_{\theta\theta(\rho)}$ = 57.599 for ν = 0.25, or $\epsilon_{\theta\theta(a)}/\epsilon_{\theta\theta(\rho)}$ = 148.263 for ν = 0.30 and their respective limiting wall ratios, b/a.

With strains as large as these, Hill's (ref 6) approximation of $\sigma_{zz} = \frac{1}{2}(\sigma_{rr}+\sigma_{\theta\theta})$ is clearly justified, except that a transitional region still exists where the material's elastic Poisson's factor is more appropriate and that a wall ratio of b/a = 8.1619 is rarely, if ever, used. For a more common wall ratio such as b/a = 2.5 or b/a = 1.4, the respective strain ratios, $\epsilon_{\theta\theta(a)}/\epsilon_{\theta\theta(\rho)}$ are 6.162 and 1.955, which barely justify Hill's approximation.

MISES' YIELD CRITERION IN A MODIFIED PLANE-STRAIN CONDITION

The above computed wall ratio, beyond which Avitzur's (ref 2) equation is not applicable (if and when 100 percent autofrettage is considered in plane-strain), is rarely used in monoblock pressure vessels. Nevertheless, it represents a mathematical limitation and questions the appropriateness of treating the material throughout the entire plastic region in a fully elastic manner (namely considering the elastically-determined Poisson's factor to prevail throughout the plastically deformed region). A compromise between the elastically-determined material's Poisson's factor at the elastic-plastic interface, r = ρ, and one that approaches Hill's suggestion of a pseudo-Poisson's factor of ν = 0.5, where the total strain is a "few times the yield point strain," is offered here. Thus, Avitzur's equation is employed with the local Poisson's factor

$$\nu_{(r)} = \nu_e + (1-\epsilon_{\theta\theta(\rho)}/\epsilon_{\theta\theta(r)}) \cdot (0.5-\nu_e) \tag{17}$$

where $\epsilon_{\theta\theta(\rho)}/\epsilon_{\theta\theta(r)}$ is derived by Eq. (16) and where ν_e is the elastically-determined Poisson's factor. Poisson's factor, $\nu_{(r)}$, derived by Eq. (17), is identical to the material's elastically-determined one at the elastic-plastic interface, r = ρ, as it should be, and it asymptotically approaches Hill's recommendation of $\nu_{(r)}$ = 0.5 as the strain ratio $\epsilon_{\theta\theta(r)}/\epsilon_{\theta\theta(\rho)} \to \infty$. Since the mathematical limitation of Avitzur's equation (Eq. (14)) is

$$|\sigma_{rr(r)}| \leq \frac{2\sqrt{1-\nu+\nu^2}}{\sqrt{3} \cdot (1-2\nu)}\ \sigma_o$$

that limit increases as ν increases, and at the limit, as $\nu \to 0.5$

$$\lim_{\nu \to 0.5} \frac{2\sqrt{1-\nu+\nu^2}}{\sqrt{3} \cdot (1-2\nu)} = \infty$$

Thus, the modified use of Eq. (14) becomes devoid of the above-mentioned mathematical limitation.

Figures 1 through 27 compare the stress distribution throughout the wall of autofrettaged thick-walled pressure vessels computed by five different methods:

1. Mises' (ref 1) in plane-stress.

2. Tresca's yield criterion.

3. (Tresca's yield criterion) $\cdot 2/\sqrt{3}$.

4. Avitzur's (ref 2) solution for a Mises' yield criterion in plane-strain.

5. Avitzur's solution for a Mises' yield criterion in a modified plane-strain with a varying Poisson's factor.

An elastically-determined Poisson factor of $\upsilon_e = 0.25$ is considered in methods #4 and #5. Figures 1 through 9 represent a vessel with a wall ratio of b/a = 1.4; Figures 10 through 18 a wall ratio of b/a = 2.5; and Figures 19 through 27 a wall ratio of b/a = 8.2. All three principal components of stress--a: tangential, b: radial, and c: axial--are represented both A: while the vessel is under (internal) pressure and B: after depressurization. Three levels of autofrettaging (penetration of the plastic region through the vessel's wall thickness) are represented:

1. $(\rho\text{-a})/(\text{b-a}) \cdot 100 = 10$ percent

2. $(\rho\text{-a})/(\text{b-a}) \cdot 100 = 50$ percent

3. $(\rho\text{-a})/(\text{b-a}) \cdot 100 = 90$ percent

In computing the stress distribution after depressurization (B), it is assumed that the recovery is fully elastic. Thus, in those cases where reverse plastic deformation is encountered upon depressurization, the approximate radius below which such a deformation takes place is marked. However, the stress distribution is not corrected accordingly. This will be investigated in the future. Furthermore, in Figures 20 through 24, 26, and 27 (50 and 90 percent autofrettage of a b/a = 8.2 tube), the first mode of deformation, Mises' yield criterion in plane-stress, is omitted since the wall ratio exceeds the limit for which this solution is applicable. As mentioned above, Mises (ref 1) has determined that in computing the stress distribution of a 100 percent autofrettaged vessel, his solution becomes unapplicable if the vessel's wall ratio b/a is greater than 2.9615. As the vessel's wall ratio increases, the percentage of autofrettaging beyond which his solution is not applicable decreases. For a tube of wall ratio b/a = 8.2, Mises' solution is not applicable when $(\rho\text{-a})/(\text{b-a}) \cdot 100 = 19.95$ percent or less than 20 percent autofrettage and beyond.

Due to the historical evolution of autofrettage as a manufacturing process, and contrary to this author's conviction, the increase in the fatigue life of an autofrettaged vessel (over that of a non-autofrettaged one) is commonly attributed to the (post-depressurization) compressive residual hoop stresses at the vessel's inner surface. If one confines his analysis of the merit of autofrettaging to the residual compressive hoop stress at the bore (as almost all investigators of the subject do--this investigator excluded) as its sole criterion, then the largest difference between the results obtained by the five different

modes of computation varies between 15 and 26 percent. The difference between results obtained through Avitzur's (ref 2) Mises' yield criterion in plane-strain solution, modified Mises' yield criterion in plane-strain, and (Tresca's yield criterion) $\cdot 2/\sqrt{3}$ computations is limited to less than ten percent (decreasing with increased vessel's wall ratio and/or with increased percent autofrettage). Furthermore, at the higher ranges (for large wall ratio vessels and at increased percent autofrettage), it is anticipated that these differences will be further reduced after correcting for reverse yielding. Therefore, one might argue that such differences do not justify the complexity and the difficulties involved in the computations according to Avitzur's (ref 2) Mises' yield criterion in plane-strain or Avitzur's modified Mises' yield criterion in plane-strain, as compared to the simplified (Tresca's yield criterion) $\cdot 2/\sqrt{3}$ method.

However, it is the conviction of this author that whether crack opening or plastic flow takes place is determined by the prevailing state of stress in its totality (and not solely as a function of a single component of stress, i.e., the hoop component, according to the prevailing thinking). Furthermore, its propagation depends on the state of stress that prevails beneath the surface. A discerning comparison between the various modes of deformation suggests that indeed there are differences in the distribution of all three principal components of stress between the various modes of computations.

Moreover, the state of stress (particularly its hydraulic component) that prevails during the plastic deformation, while the vessel is being pressurized, determines whether pre-existing microcracks and/or microvoids will grow or heal in the process. This parameter is not represented by the retained stresses, and hence, any comparison of the latter values, as obtained by the five different methods, is devoid of such information.

The most important point to be considered is that the process itself is neither in plane-stress nor in plane-strain. Whether and/or in what range the two Avitzur's solutions differ significantly from the simplified (Tresca's yield criterion) $\cdot 2/\sqrt{3}$ solution, should be determined only after the former are adjusted for free ends (general plane-strain) condition that prevail during fluid autofrettage or adjusted for the axial load that prevails during mandrel autofrettage. A clue to the significance of the anticipated differences between these three methods of calculations when the above corrections are made can be seen by comparing the distributions of the axial stress component in plane-strain.

In very long pressure vessels (i.e., in gun tubes), calculating the axial component of the retained stress is important due to its effect on the vessel's straightness and/or on a post-autofrettage straightening operation. However, that is beyond the scope of this work.

CONCLUSIONS

Inherent to Avitzur's (ref 2) solution for the stress distribution in pressurized thick-walled vessels in plane-strain, there is a wall ratio beyond which it is mathematically unapplicable. A modification to that method is proposed here. This mathematical limitation is compared to a similar limitation that Mises' (ref 1) pointed out to restrict the applicability of this solution in plane-stress. The numerical results obtained by each of these methods of calculation are compared to each other as well as to those obtained by assuming that Tresca's yield criterion prevails (either with the material's own yield strength, σ_0, or with a yield strength of $2/\sqrt{3}\ \sigma_0$ often misrepresented as Mises' yield criterion in plane-strain). The most significant difference is in the axial stress component, which only Avitzur's (ref 2) solution and its modified version, as well as (Tresca's yield criterion) $\cdot 2/\sqrt{3}$ offer.

REFERENCES

1. R. von Mises, "Mechanik der Fasten Köpper im Plastich Deformablen Zustand," *Nachrichten der Gesellschaft der Wisseschaften Gottingen*, 1913, pp. 582-592.

2. B. Avitzur, "Autofrettage--Stress Distribution Under Load and Retained Stresses After Depressurization," ARCCB-TR-92032, Benet Laboratories, Watervliet, NY, July 1992.

3. S. Timoshenko and J.N. Goodier, *Theory of Elasticity*, Second Edition, Engineering Society Monographs, 1951.

4. W.R.D. Manning, "The Overstrain of Tubes by Internal Pressure," *Engineering*, Vol. 159, 1945, pp. 101-102 and 183-184.

5. T.E. Davidson, Dr. C.S.Barton, A.N. Reiner, and D.P. Kendall, "A New Approach to the Autofrettage of High Strength Gun Tubes," WVT-RI-5901, Watervliet Arsenal, Watervliet, NY, April 1959.

6. R. Hill, *The Mathematical Theory of Plasticity*, The Oxford Engineering Science Service, 1956, pp. 78-79.

7. A. Stacey and G.A. Webster, "Determination of Residual Stress Distribution in Autofrettaged Tubing," *International Journal of Pressure Vessels and Piping*, Vol. 31, 1988, pp. 205-220.

8. B. Avitzur, "Determination of Residual Stress Distribution in Autofrettaged Tubing: A Discussion," ARCCB-MR-88034, Benet Laboratories, Watervliet, NY, August 1988; also in: *International Journal of Pressure Vessels and Piping*, Vol. 38, No. 2, 1989, pp. 147-157.

9. B. Avitzur, "Stress Distribution in Concentrically-Hollowed Thick-Wall Tubes Subjected to Uniform Radial Loading," Benet Laboratories, Watervliet, NY, to be published.

APPENDIX A

HOOP STRAIN IN THE PLASTICALLY DEFORMED REGION

Volume conservation within the plastically deformed region can be expressed as

$$\frac{\pi}{4}(\rho^2 - r^2) = \frac{\pi}{4}\left[(1+\epsilon_{\theta\theta(\rho)})^2 \cdot \rho^2 - (1+\epsilon_{\theta\theta(r)})^2 \cdot r^2\right]$$

Thus,

$$\epsilon^2_{\theta\theta(r)} + 2\epsilon_{\theta\theta(r)} - (2\epsilon_{\theta\theta(\rho)} + \epsilon^2_{\theta\theta(\rho)})\left(\frac{\rho}{r}\right)^2 = 0$$

Hence,

$$\epsilon_{\theta\theta(r)} = -1 \pm \sqrt{1 + (2\epsilon_{\theta\theta(\rho)} + \epsilon^2_{\theta\theta(\rho)})\left(\frac{\rho}{r}\right)^2}$$

or

$$\epsilon_{\theta\theta(r)} = \sqrt{1 + (2 + \epsilon_{\theta\theta(\rho)}) \cdot \epsilon_{\theta\theta(\rho)} \cdot \left(\frac{\rho}{r}\right)^2} - 1$$

APPENDIX B

COMPUTATION OF THE MAXIMUM PLASTIC REGION, ρ/a, FOR WHICH AVITZUR'S EQUATION IS APPLICABLE

Avitzur's solution (refs 2,8) in plane-strain reads

$$\ln\frac{r}{\rho} = -\tfrac{1}{4}\left\{\ln\frac{\left[\sqrt{\frac{3}{\eta}}\cdot\sqrt{\frac{4\delta}{3\eta}\frac{\delta}{\eta}\left(\frac{\sigma_o}{\sigma_{rr(r)}}\right)^2-1}+1\right]^2}{4\frac{\delta}{\eta^2}\left(\frac{\sigma_o}{\sigma_{rr(r)}}\right)^2} - \ln\frac{(3+\eta)\left(\frac{b}{\rho}\right)^4}{3\left(\frac{b}{\rho}\right)^4+\eta}\right.$$

$$\left.-2\sqrt{\frac{3}{\eta}}\cdot\left[\tan^{-1}\sqrt{\frac{4\delta}{3\eta}\left(\frac{\sigma_o}{\sigma_{rr(r)}}\right)^2-1}-\tan^{-1}\frac{3\left(\frac{b}{\rho}\right)+\eta}{\sqrt{3\eta}\left[\left(\frac{b}{\rho}\right)^2-1\right]}\right]\right\}$$

Thus, at the limit of its applicability

$$|\sigma_{rr(a)}| = 2\sqrt{\frac{\delta}{3\eta}}\cdot\sigma_o$$

for which

$$\left(\frac{\sigma_o}{\sigma_{rr(a)}}\right)^2 = \frac{3\eta}{4\delta}\quad,\quad\sqrt{\frac{4\delta}{3\eta}\left(\frac{\sigma_o}{\sigma_{rr(a)}}\right)^2-1} = 0$$

and

$$\frac{\left[\sqrt{\frac{3}{\eta}}\cdot\sqrt{\frac{4\delta}{3\eta}\left(\frac{\sigma_o}{\sigma_{rr(a)}}\right)^2-1}+1\right]^2}{4\frac{\delta}{\eta^2}\left(\frac{\sigma_o}{\sigma_{rr(a)}}\right)^2} = \frac{\eta}{3}$$

Also, from Eq. (12a) at $r = \rho$

$$\left(\frac{\sigma_o}{\sigma_{rr(\rho)}}\right)^2 = \frac{3\left(\frac{b}{\rho}\right)^4 + \eta}{\left[\left(\frac{b}{\rho}\right)^2 - 1\right]^2}$$

Hence,

$$\sqrt{\frac{4\delta}{3\eta}\left(\frac{\sigma_o}{\sigma_{rr(\rho)}}\right)^2 - 1} = \frac{3\left(\frac{b}{\rho}\right)^2 + \eta}{\sqrt{3\eta}\left[\left(\frac{b}{\rho}\right)^2 - 1\right]}$$

or

$$\frac{\left[\sqrt{\frac{3}{\eta}} \cdot \sqrt{\frac{4\delta}{3\eta}\left(\frac{\sigma_o}{\sigma_{rr(\rho)}}\right)^2 - 1} + 1\right]^2}{4\frac{\delta}{\eta^2}\left(\frac{\sigma_o}{\sigma_{rr(\rho)}}\right)^2} = \frac{4\delta \cdot \left(\frac{b}{\rho}\right)^4}{3\left(\frac{b}{\rho}\right)^4 + \eta}$$

from which

$$\ln\frac{\rho}{a} = \frac{1}{4}\left\{\ln\frac{\eta}{3} - \ln\frac{4\delta\left(\frac{b}{\rho}\right)^4}{3\left(\frac{b}{\rho}\right)^4 + \eta} - 2 \cdot \sqrt{\frac{3}{\eta}} \cdot \left[\tan^{-1}(0) - \tan^{-1}\frac{3\left(\frac{b}{\rho}\right)^2 + \eta}{\sqrt{3\eta}\left[\left(\frac{b}{\rho}\right)^2 - 1\right]}\right]\right\}$$

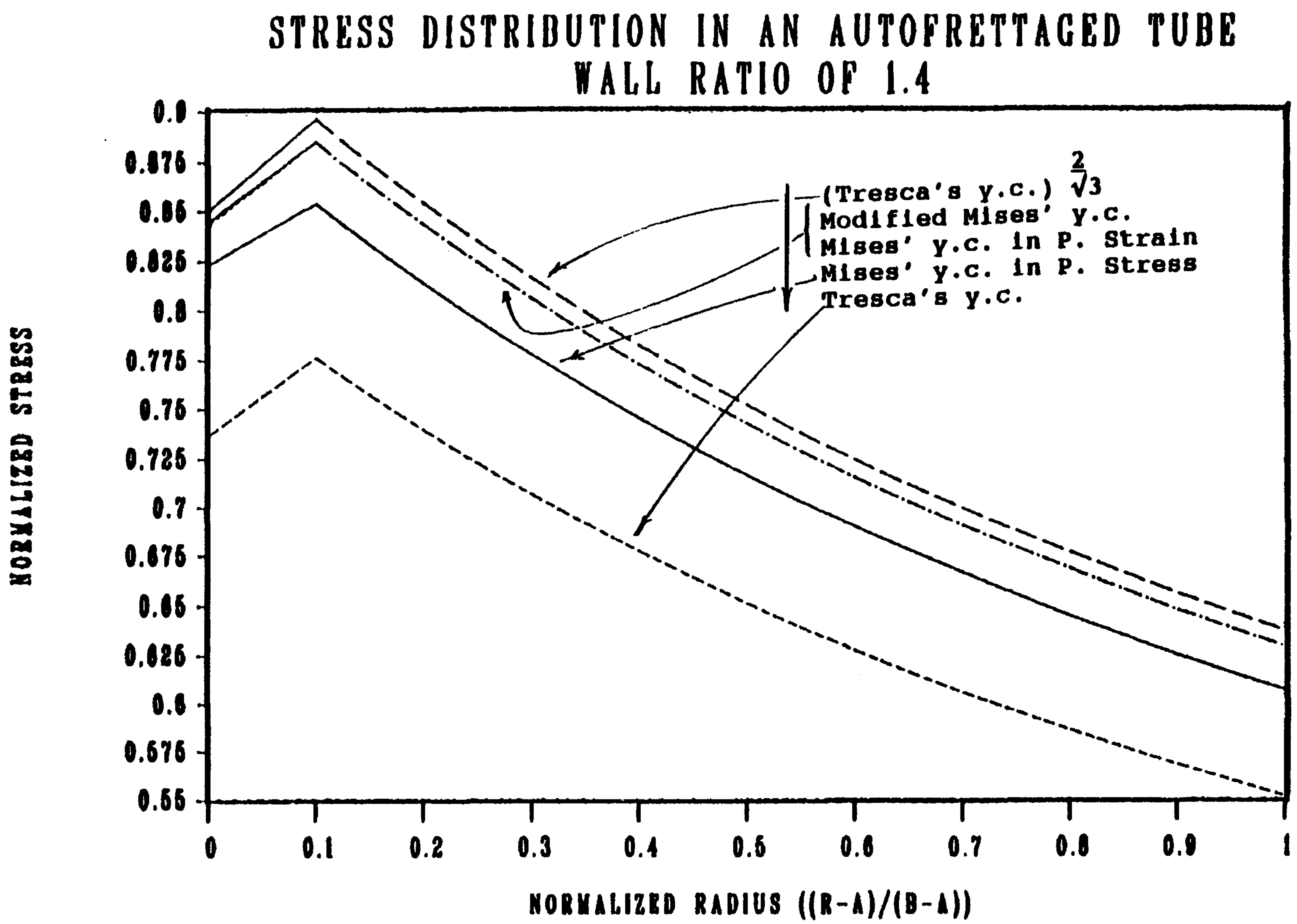

Figure 1a. **Tangential stress component:** Stress distribution in an autofrettaged pressure vessel with a wall ratio of b/a = 1.4 under (autofrettaging) pressure of 10 percent autofrettage.

STRESS DISTRIBUTION IN AN AUTOFRETTAGED TUBE WALL RATIO OF 1.4

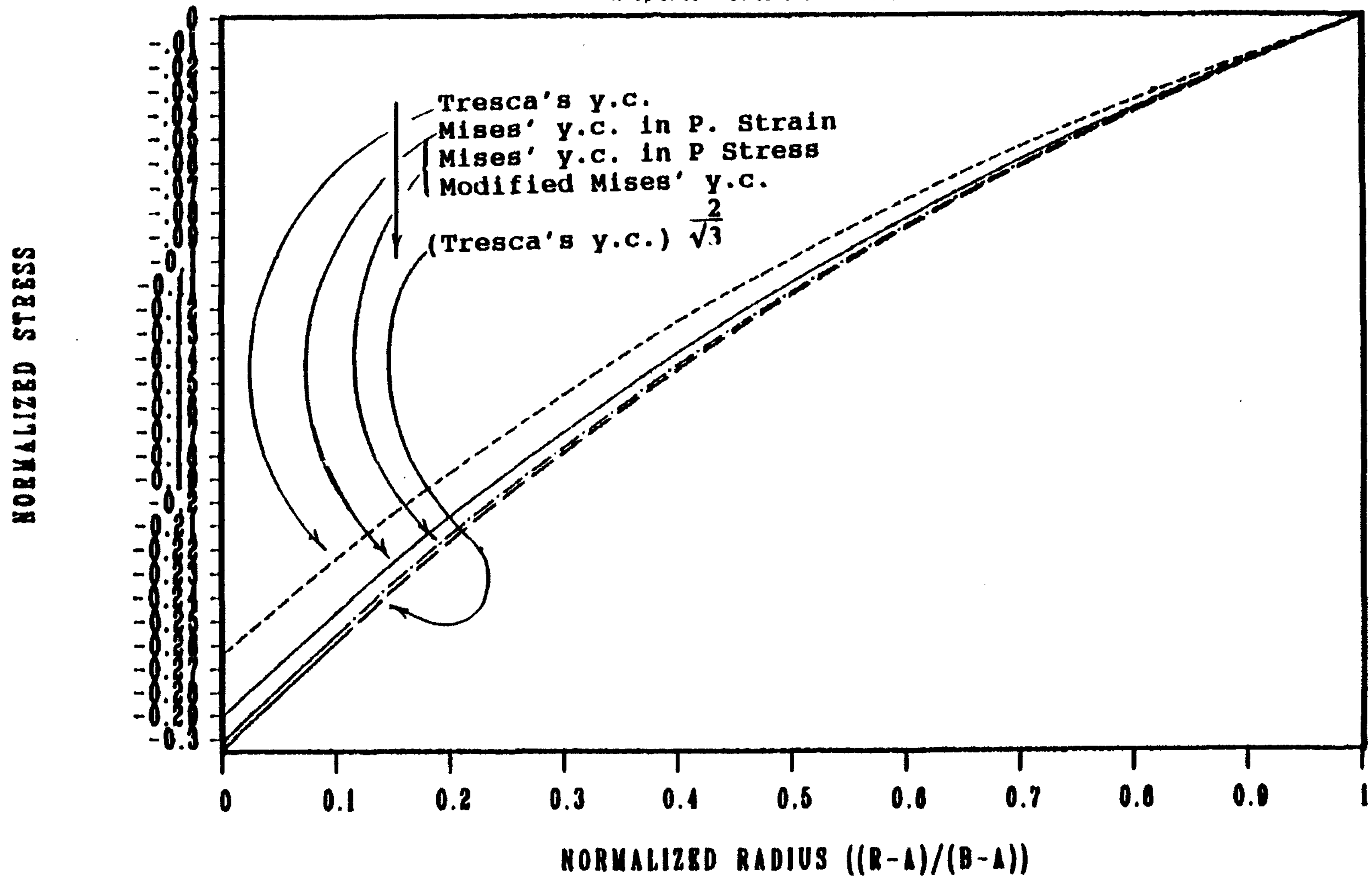

Figure 1b. **Radial stress component:** Stress distribution in an autofrettaged pressure vessel with a wall ratio of b/a = 1.4 under (autofrettaging) pressure of 10 percent autofrettage.

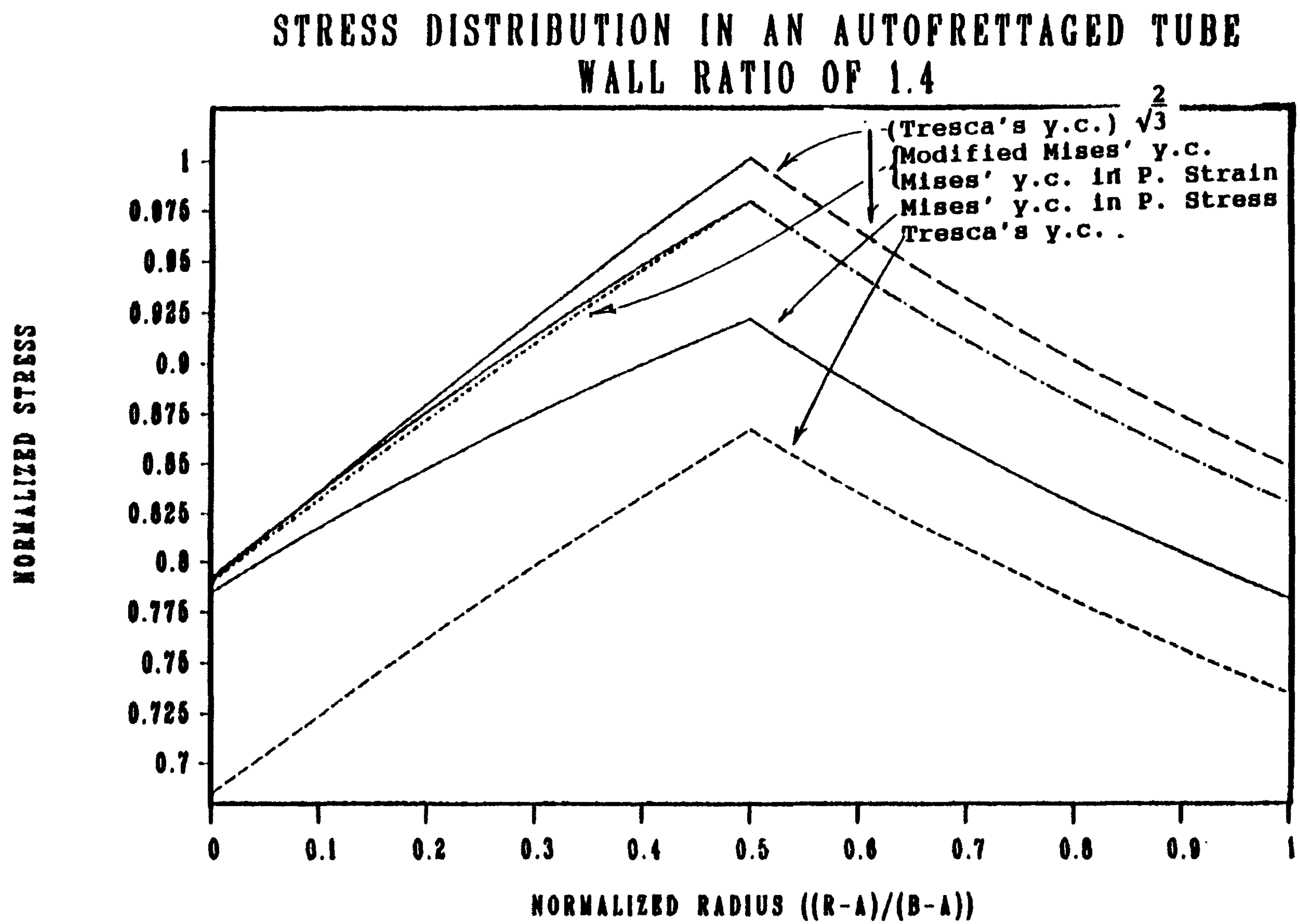

Figure 2a. **Tangential stress component**: Stress distribution in an autofrettaged pressure vessel with a wall ratio of b/a = 1.4 under (autofrettaging) pressure of 50 percent autofrettage.

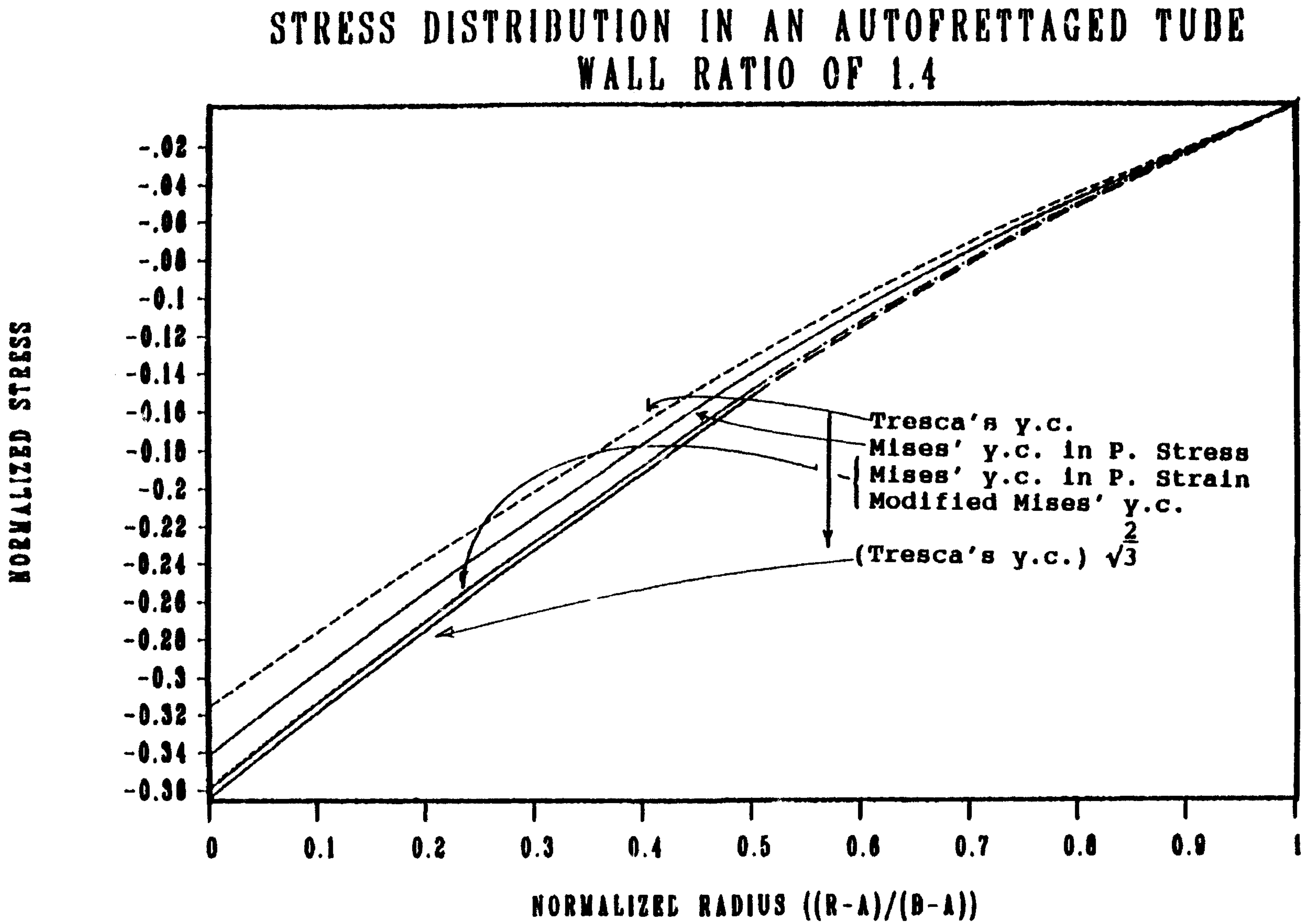

Figure 2b. **Radial stress component:** Stress distribution in an autofrettaged pressure vessel with a wall ratio of b/a = 1.4 under (autofrettaging) pressure of 50 percent autofrettage.

STRESS DISTRIBUTION IN AN AUTOFRETTAGED TUBE
WALL RATIO OF 1.4

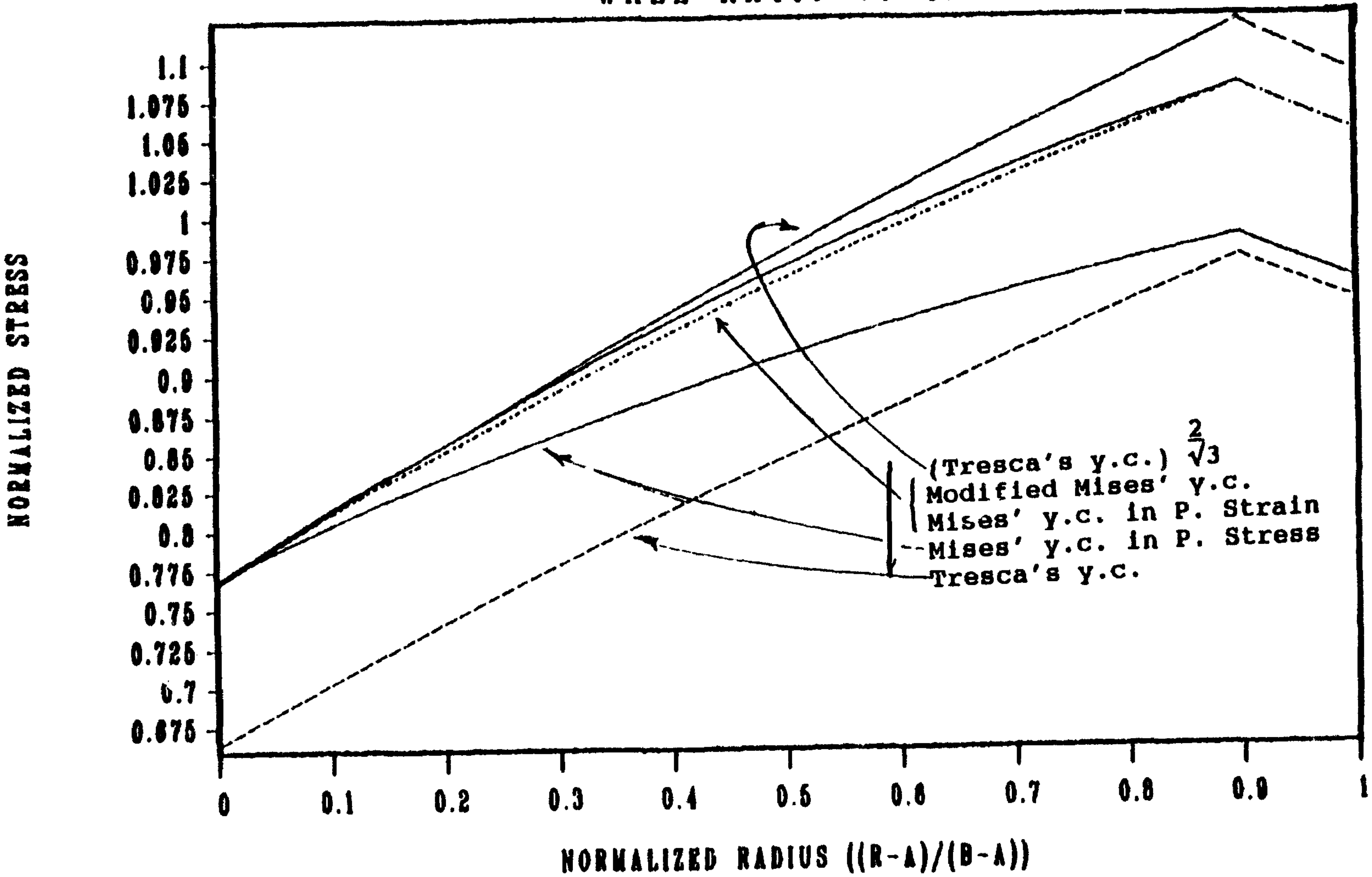

Figure 3a. **Tangential stress component:** Stress distribution in an autofrettaged pressure vessel with a wall ratio of b/a = 1.4 under (autofrettaging) pressure of 90 percent autofrettage.

18

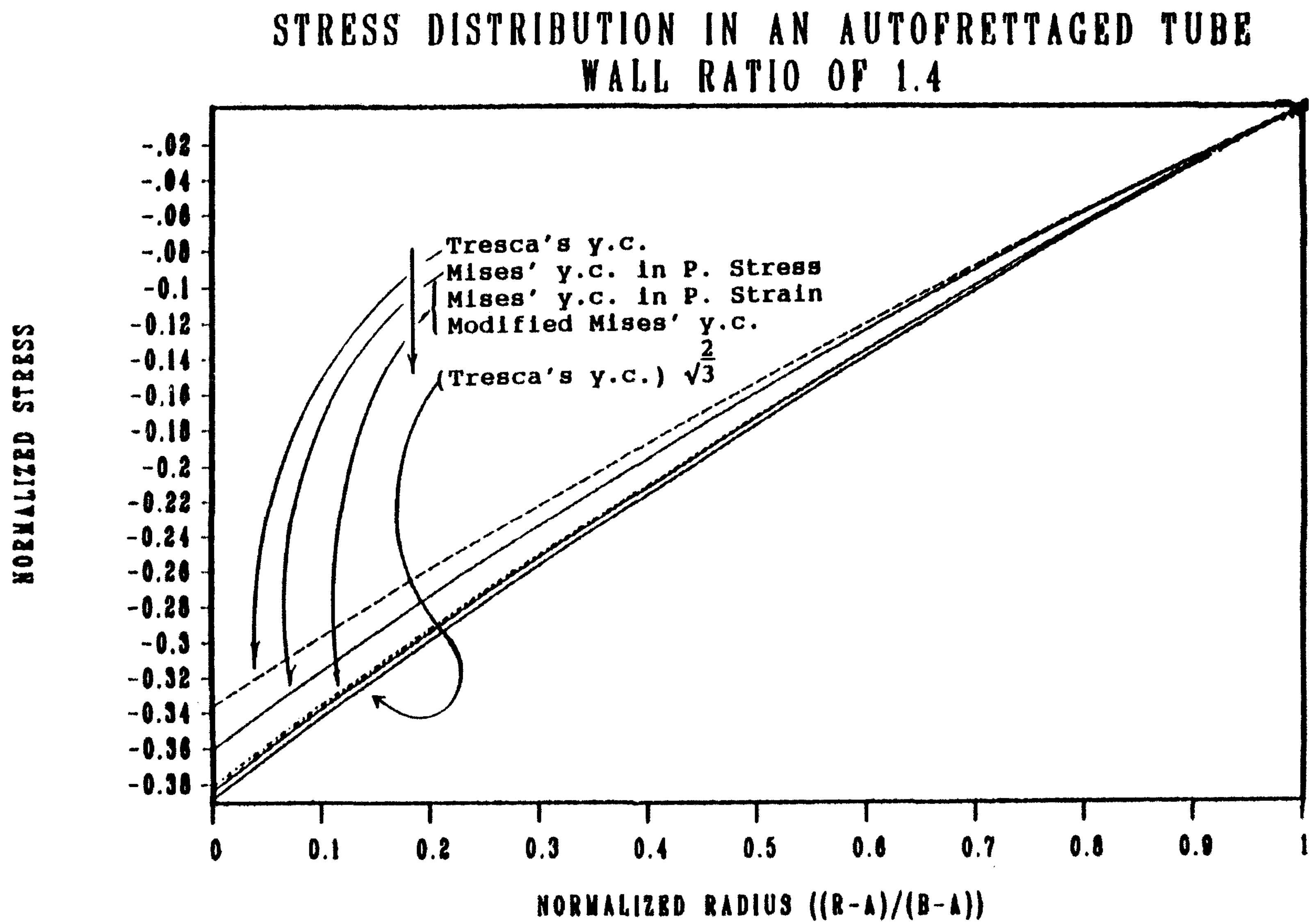

Figure 3b. **Radial stress component**: Stress distribution in an autofrettaged pressure vessel with a wall ratio of b/a = 1.4 under (autofrettaging) pressure of 90 percent autofrettage.

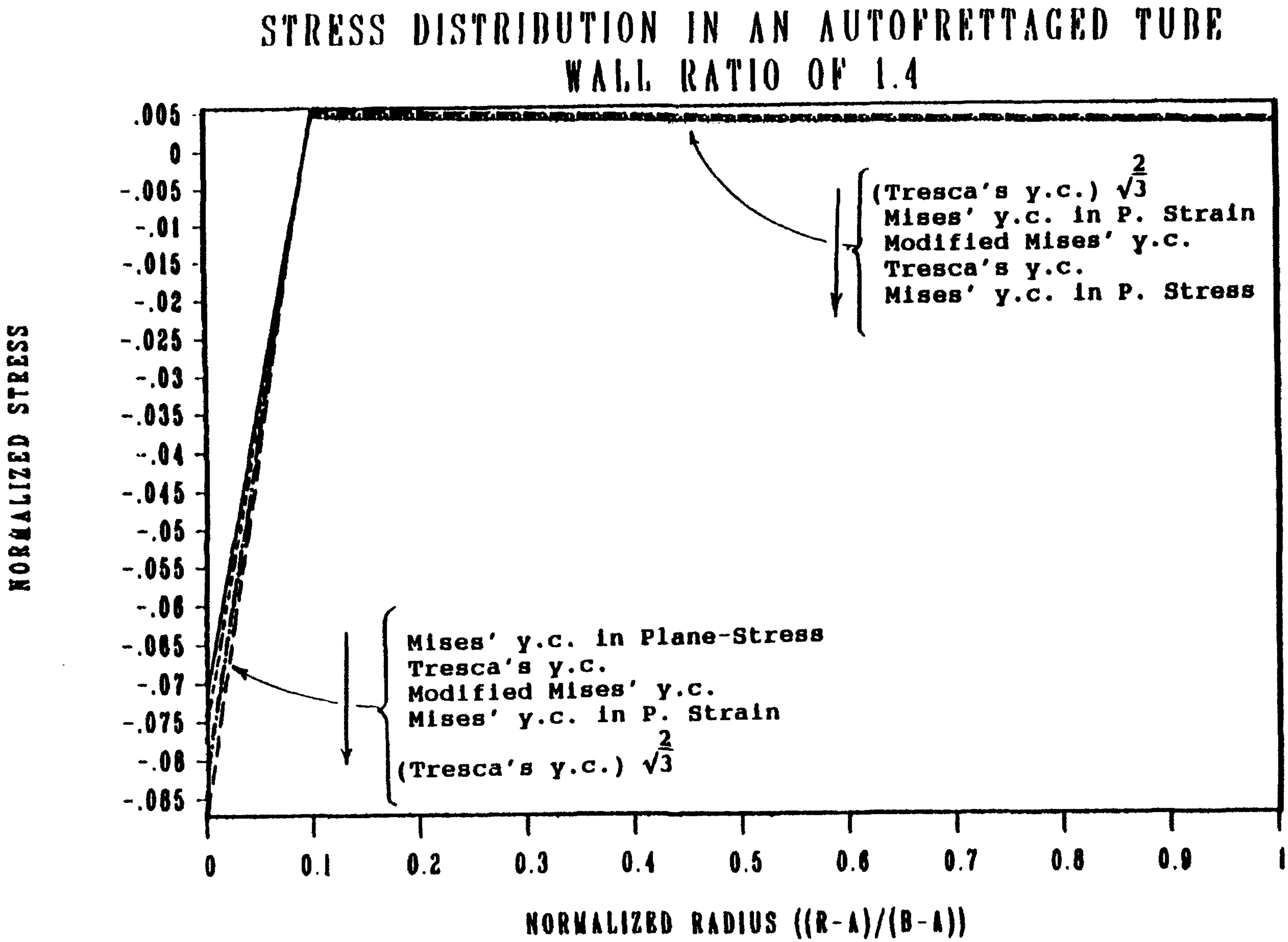

Figure 4a. **Tangential stress component**: Stress distribution in an autofrettaged pressure vessel with a wall ratio of b/a = 1.4 after depressurization of 10 percent autofrettage.

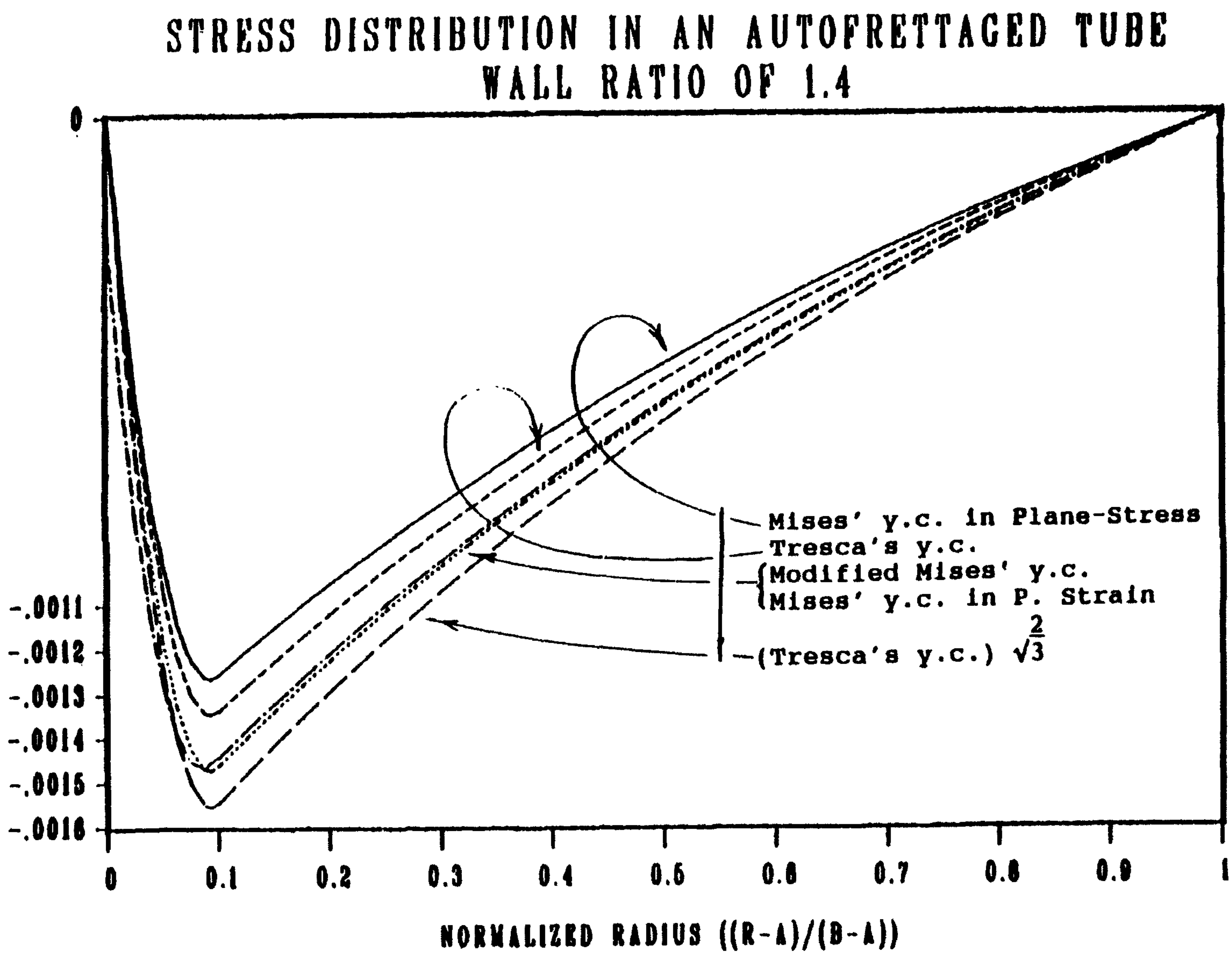

Figure 4b. **Radial stress component:** Stress distribution in an autofrettaged pressure vessel with a wall ratio of b/a = 1.4 after depressurization of 10 percent autofrettage.

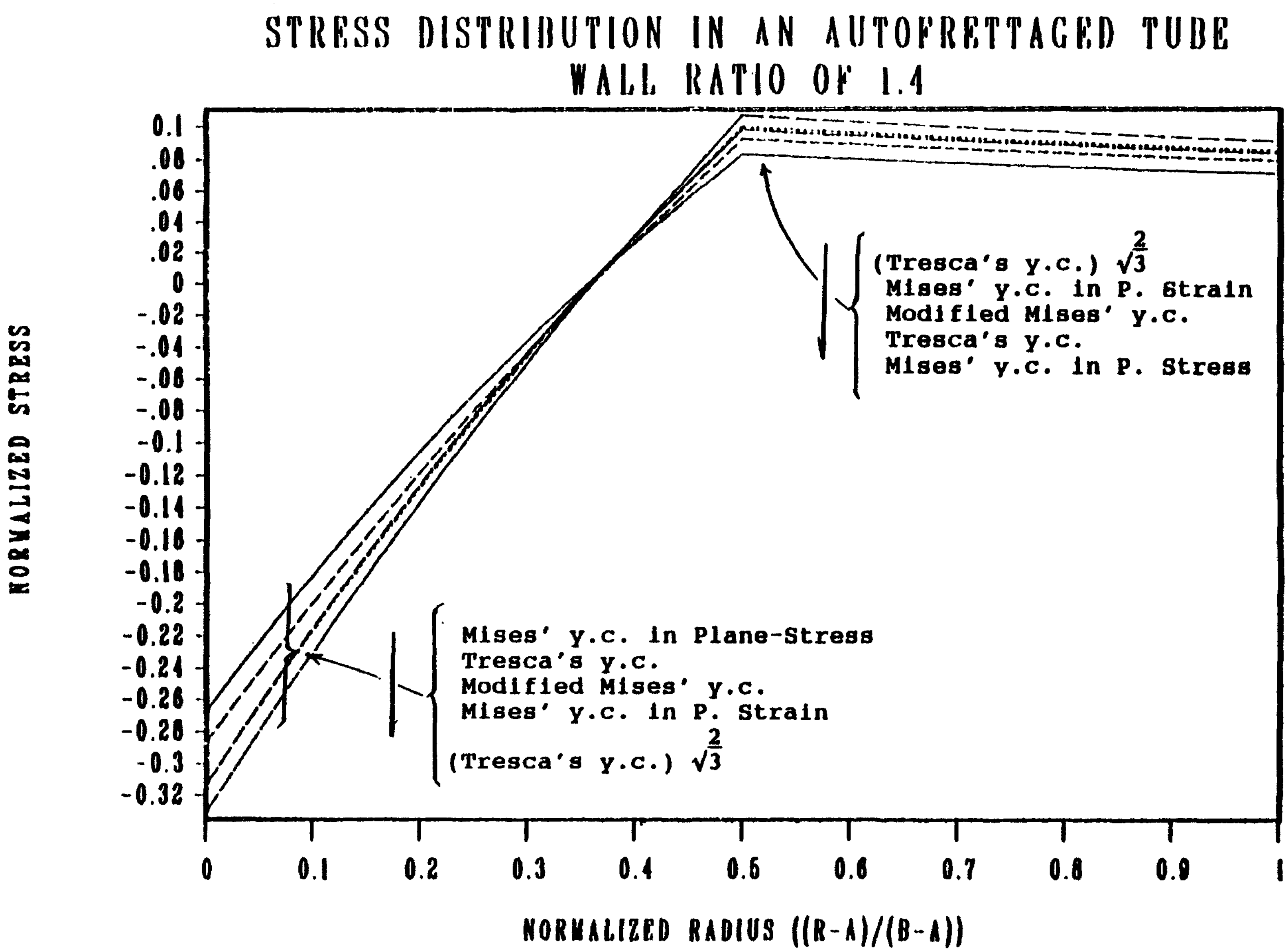

Figure 5a. **Tangential stress component:** Stress distribution in an autofrettaged pressure vessel with a wall ratio of b/a = 1.4 after depressurization of 50 percent autofrettage.

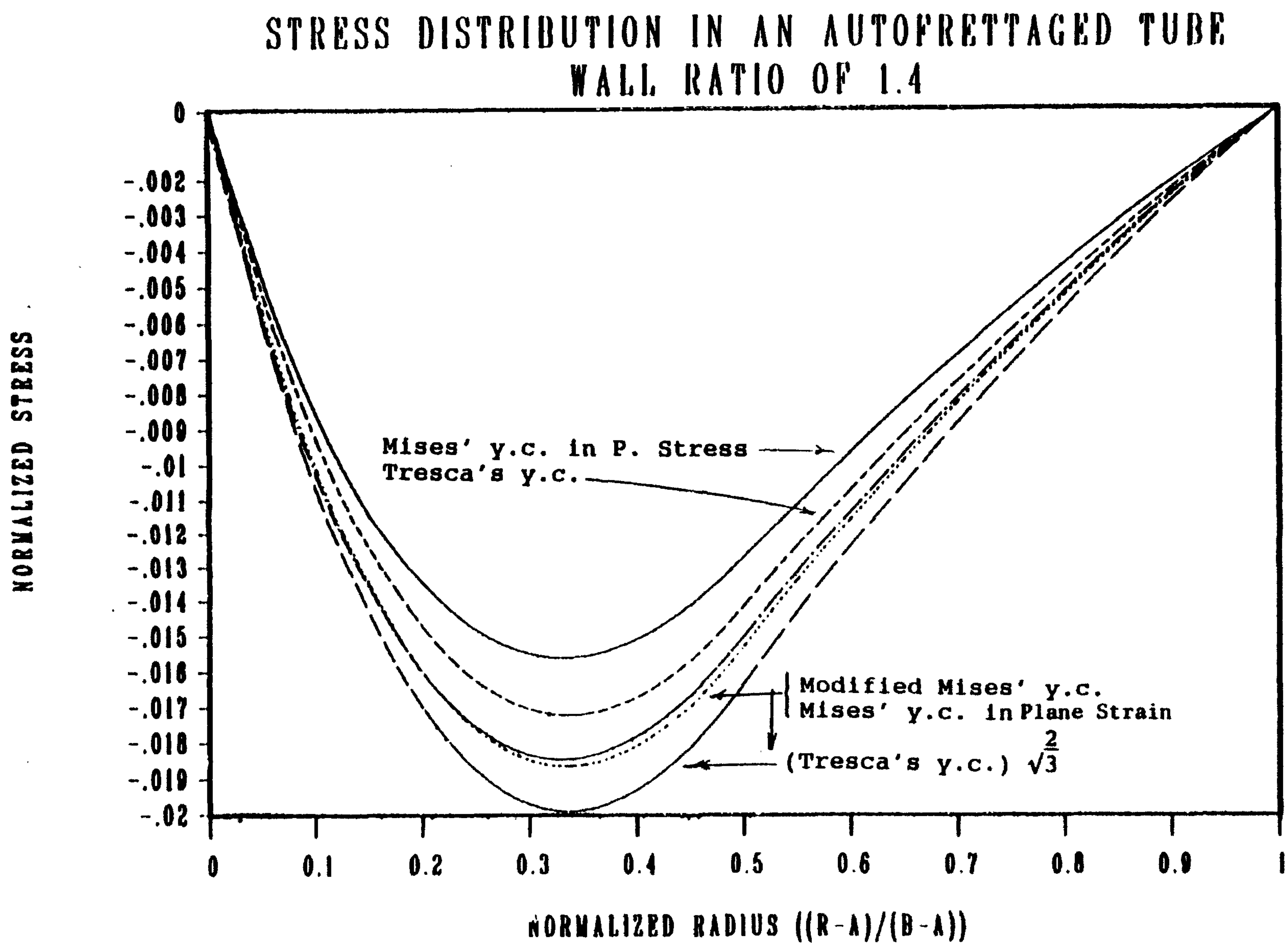

Figure 5b. **Radial stress component**: Stress distribution in an autofrettaged pressure vessel with a wall ratio of b/a = 1.4 after depressurization of 50 percent autofrettage.

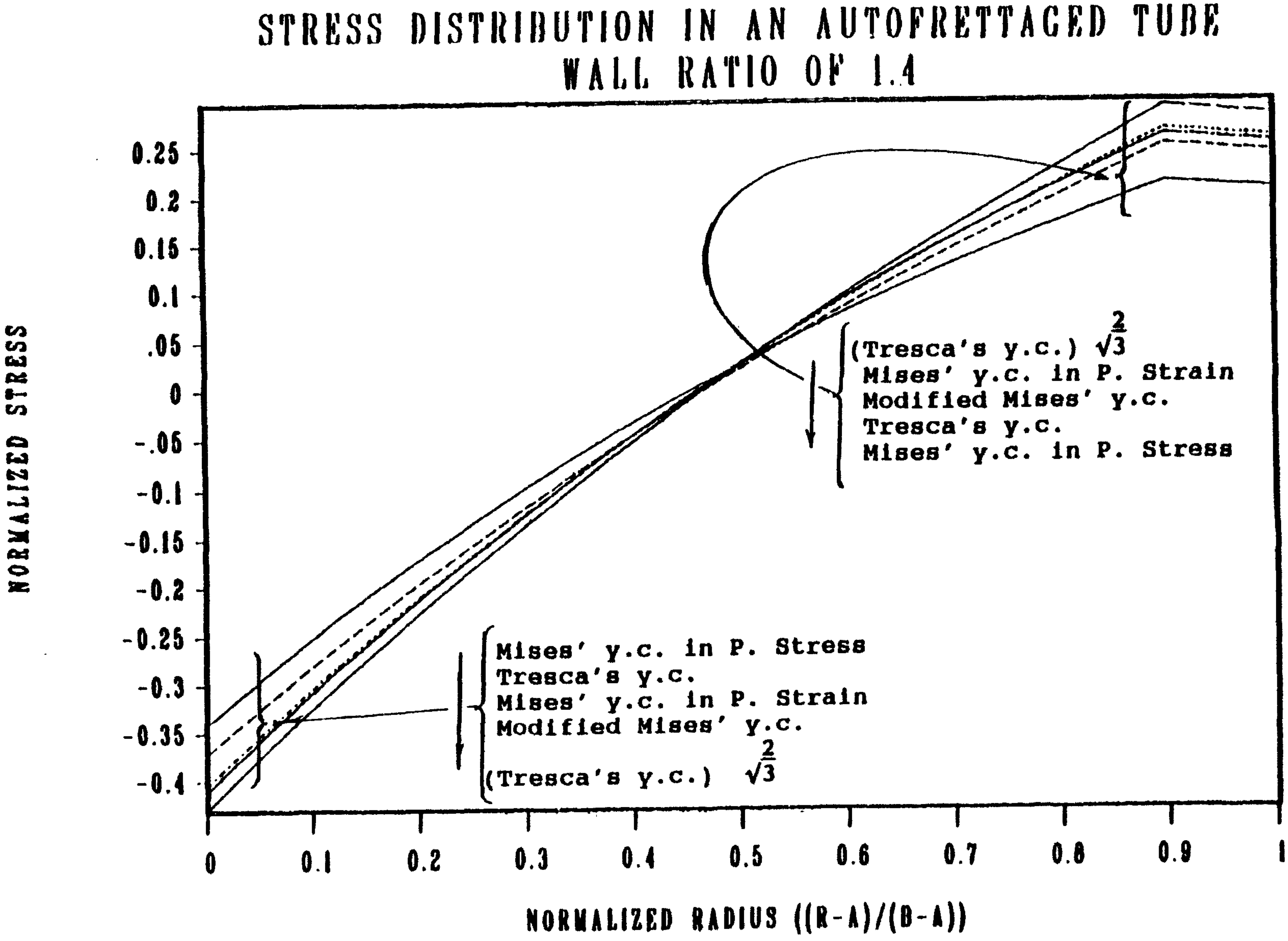

Figure 6a. **Tangential stress component:** Stress distribution in an autofrettaged pressure vessel with a wall ratio of b/a = 1.4 after depressurization of 90 percent autofrettage.

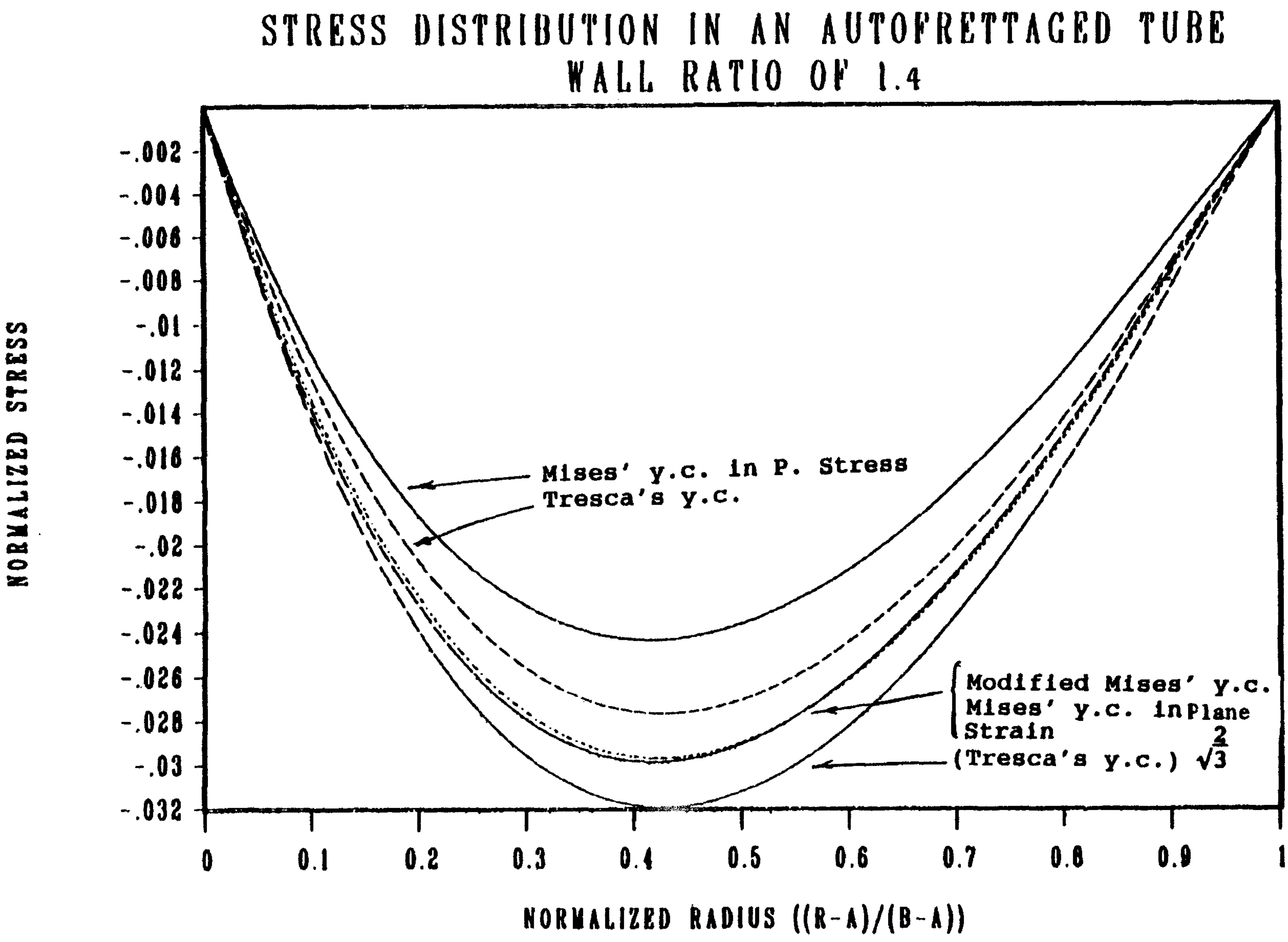

Figure 6b. **Radial stress component**: Stress distribution in an autofrettaged pressure vessel with a wall ratio of b/a = 1.4 after depressurization of 90 percent autofrettage.

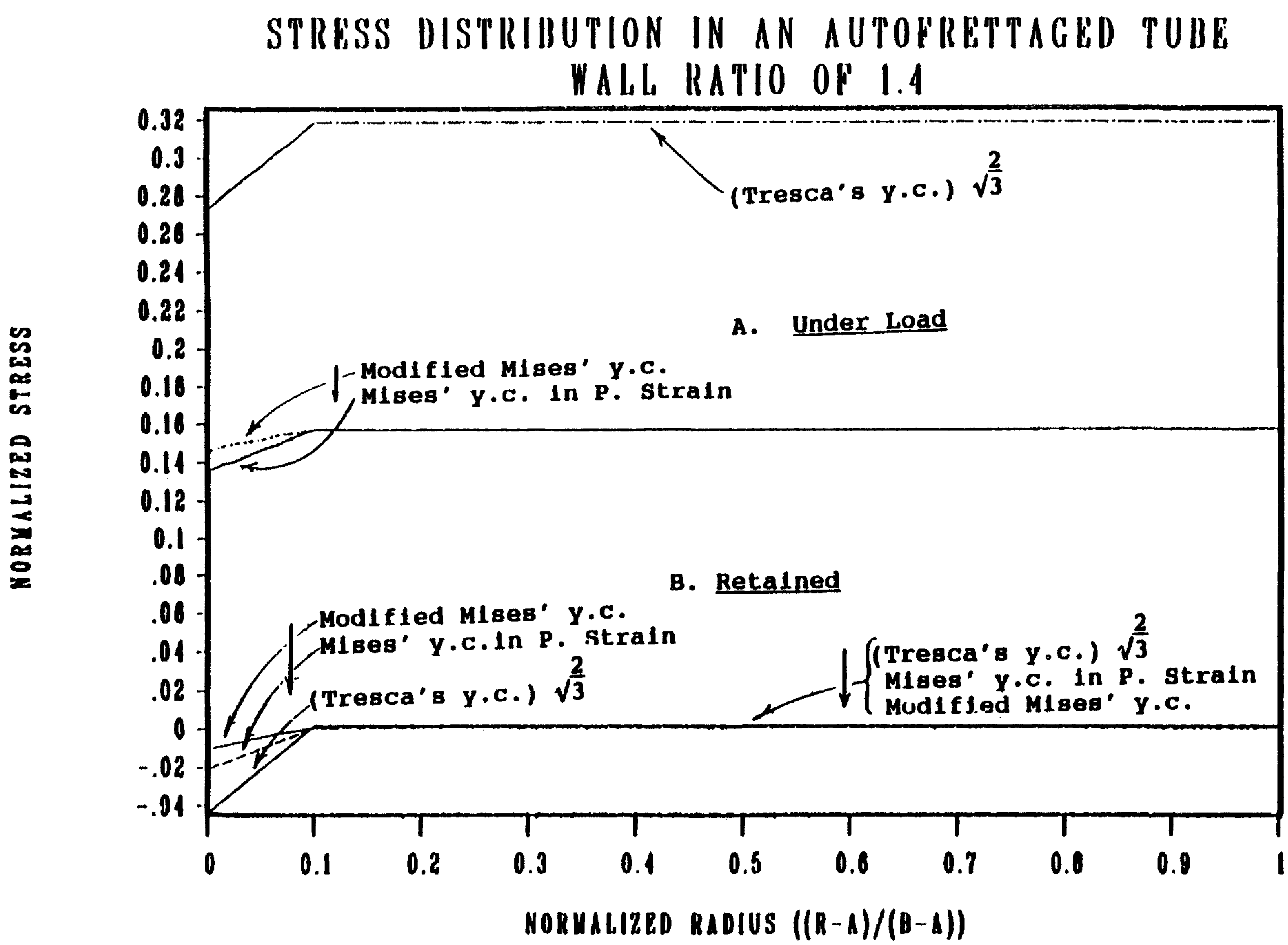

Figure 7. **Axial stress component**: Stress distribution in an autofrettaged pressure vessel with a wall ratio of b/a = 1.4 under (autofrettaging) pressure and after depressurization of 10 percent autofrettage.

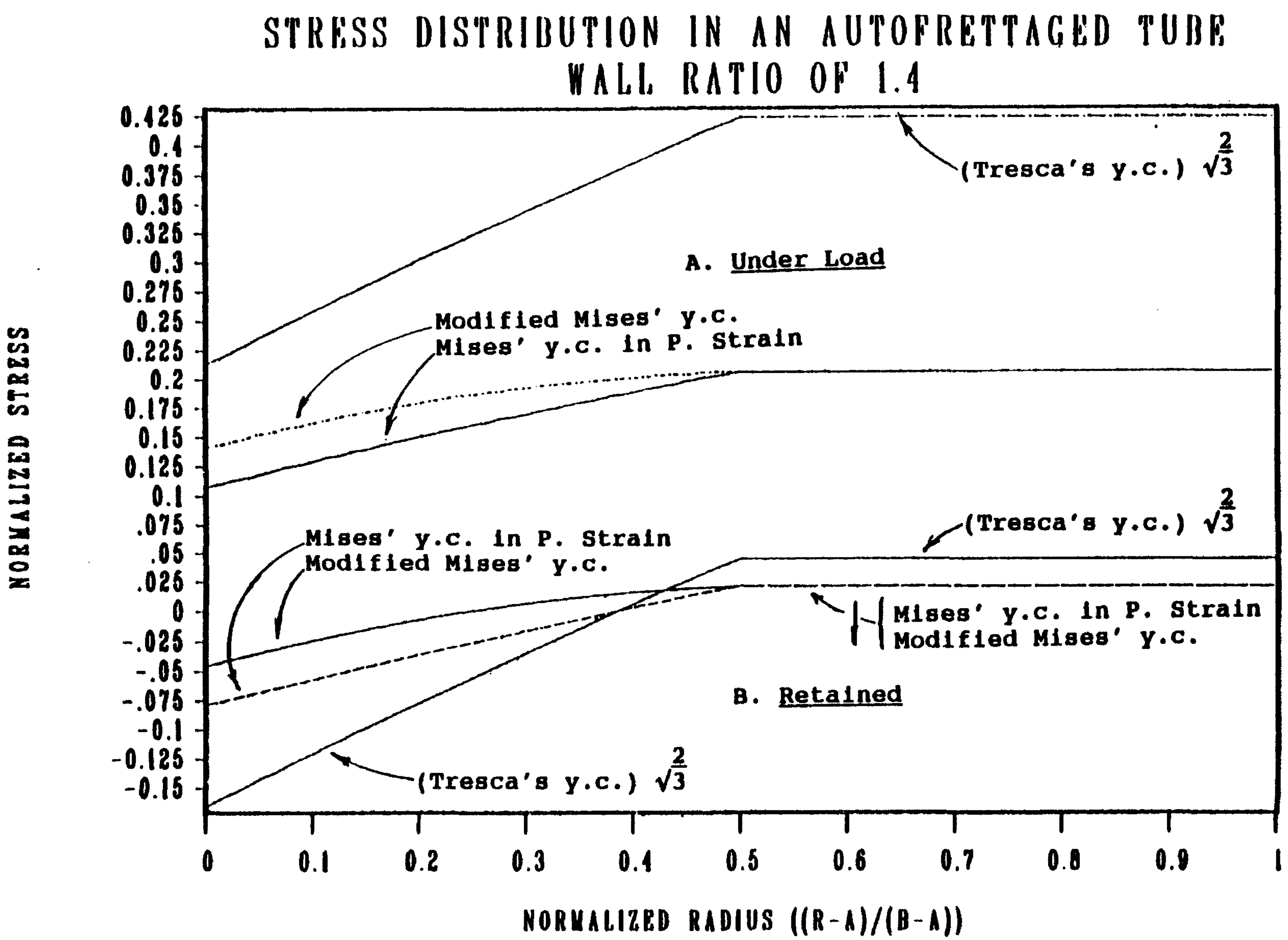

Figure 8. **Axial stress component:** Stress distribution in an autofrettaged pressure vessel with a wall ratio of b/a = 1.4 under (autofrettaging) pressure and after depressurization of 50 percent autofrettage.

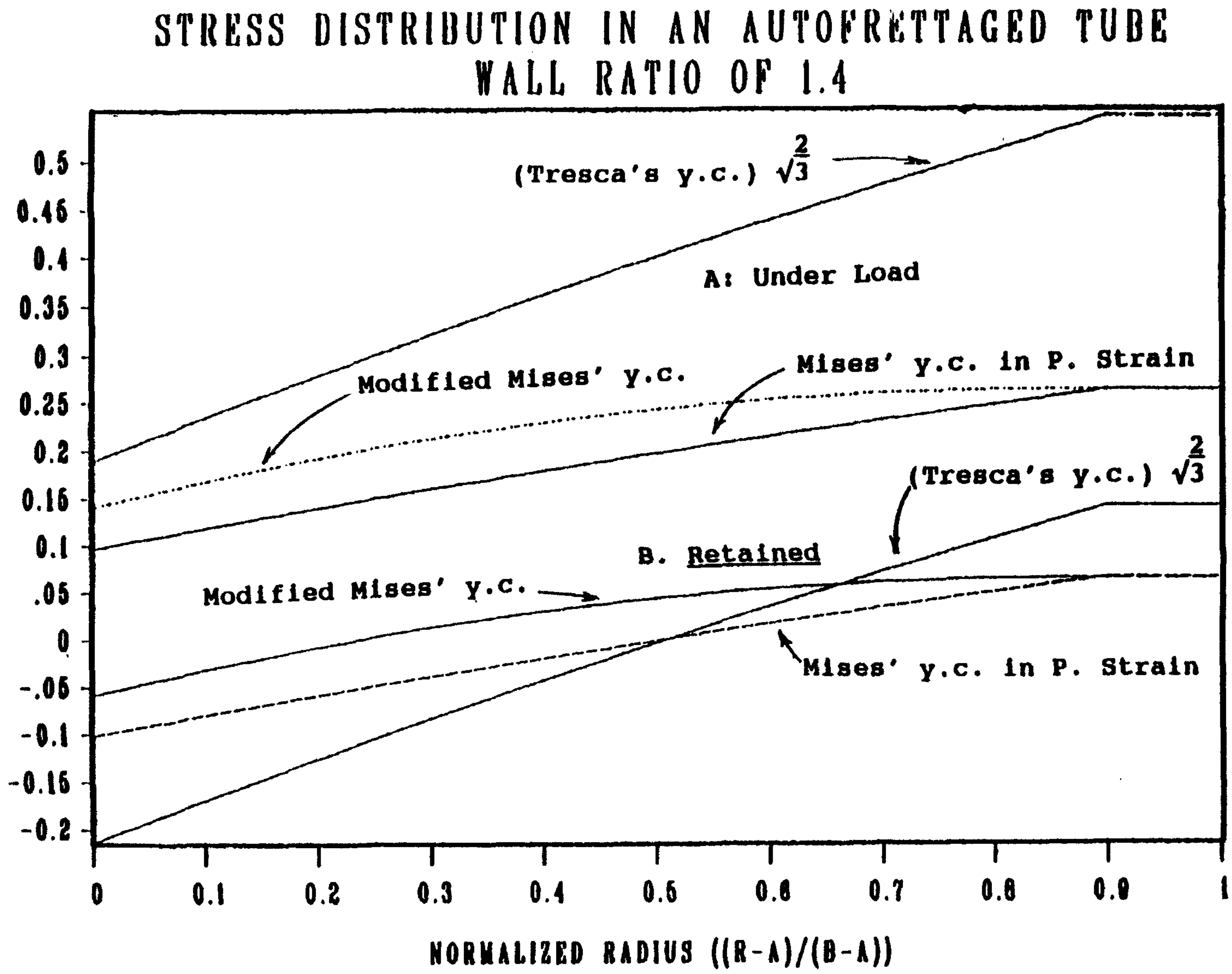

Figure 9. **Axial stress component:** Stress distribution in an autofrettaged pressure vessel with a wall ratio of b/a = 1.4 under (autofrettaging) pressure and after depressurization of 90 percent autofrettage.

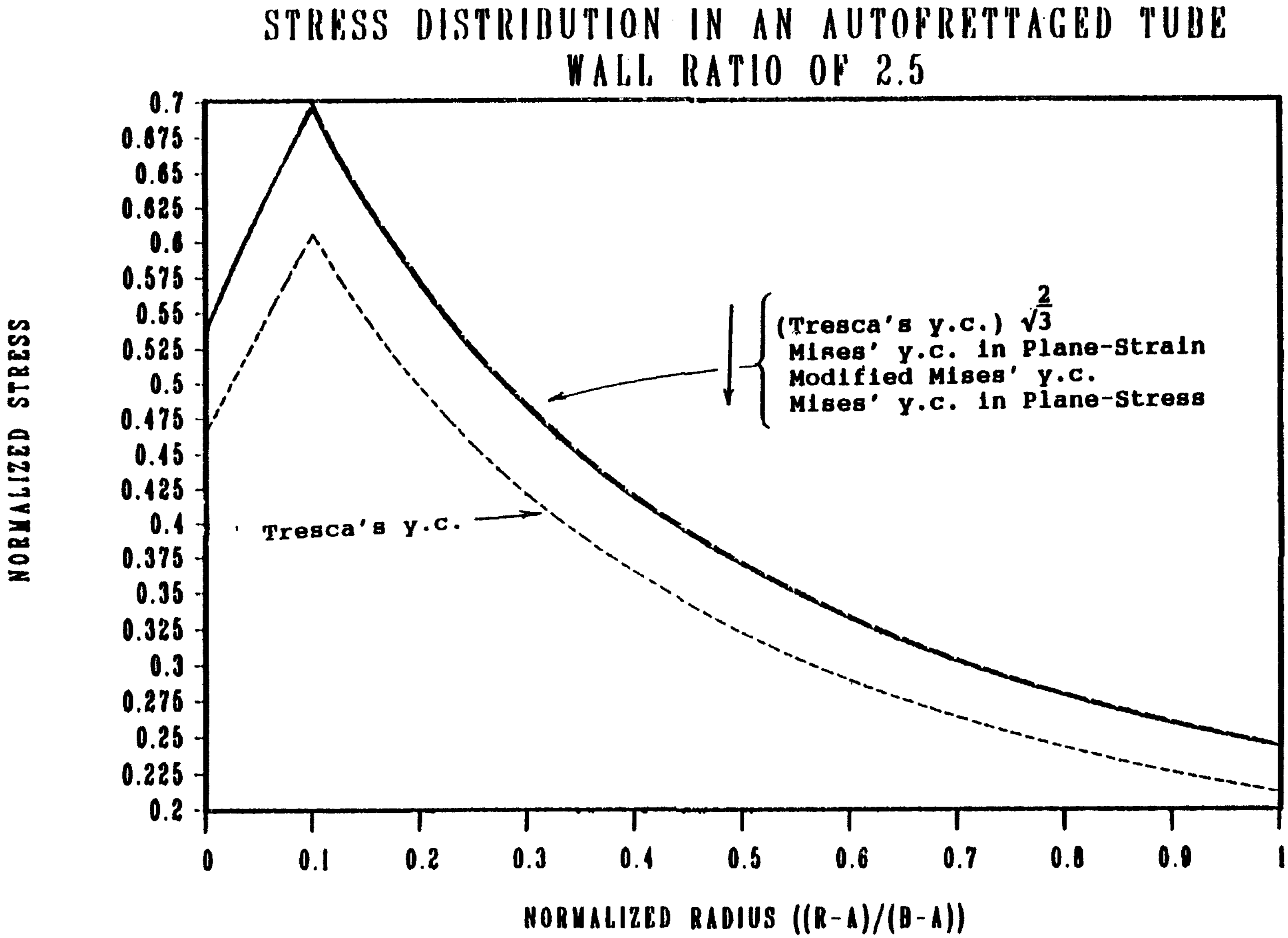

Figure 10a. **Tangential stress component**: Stress distribution in an autofrettaged pressure vessel with a wall ratio of b/a = 2.5 under (autofrettaging) pressure of 10 percent autofrettage.

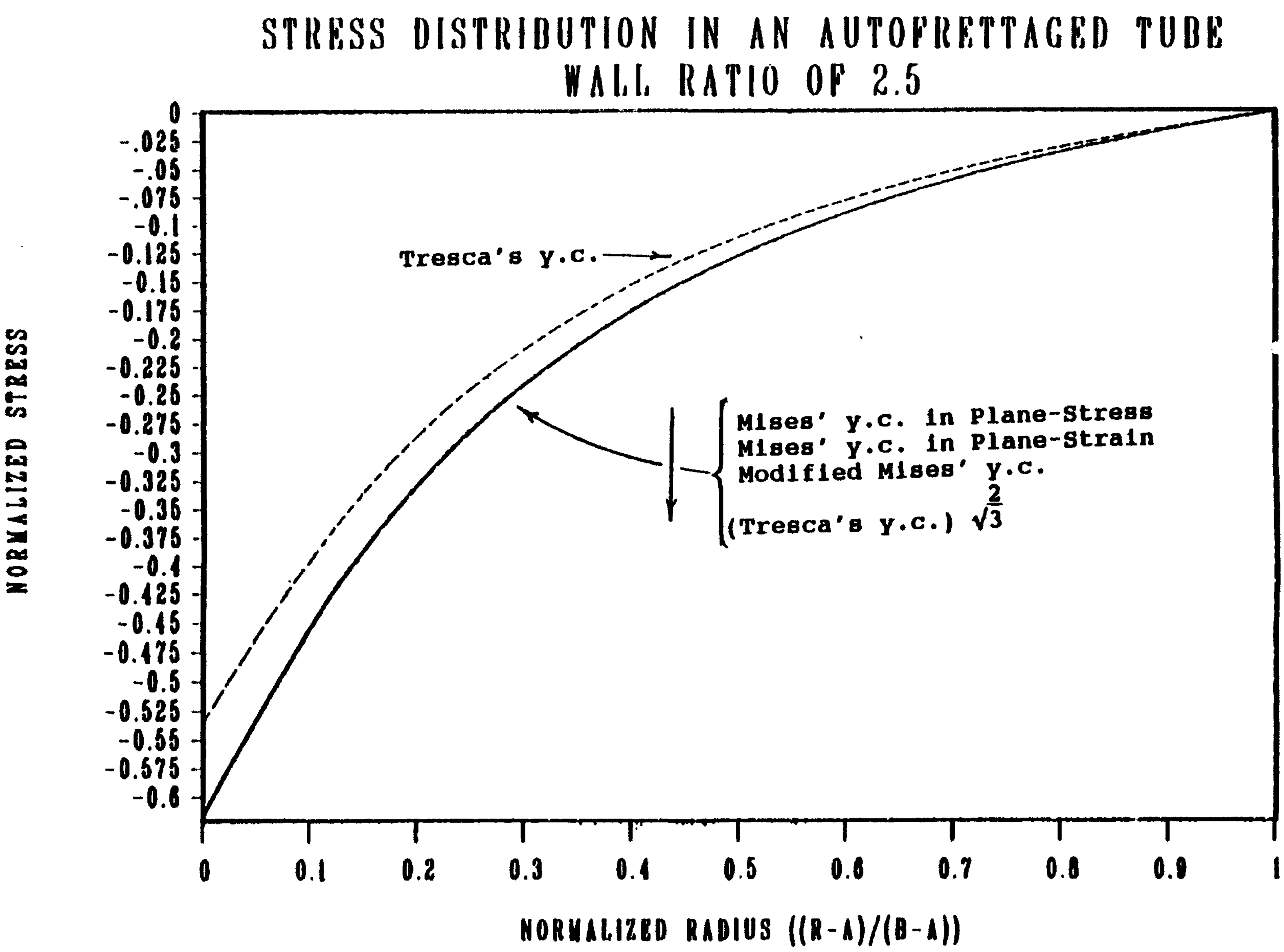

Figure 10b. **Radial stress component**: Stress distribution in an autofrettaged pressure vessel with a wall ratio of b/a = 2.5 under (autofrettaging) pressure of 10 percent autofrettage.

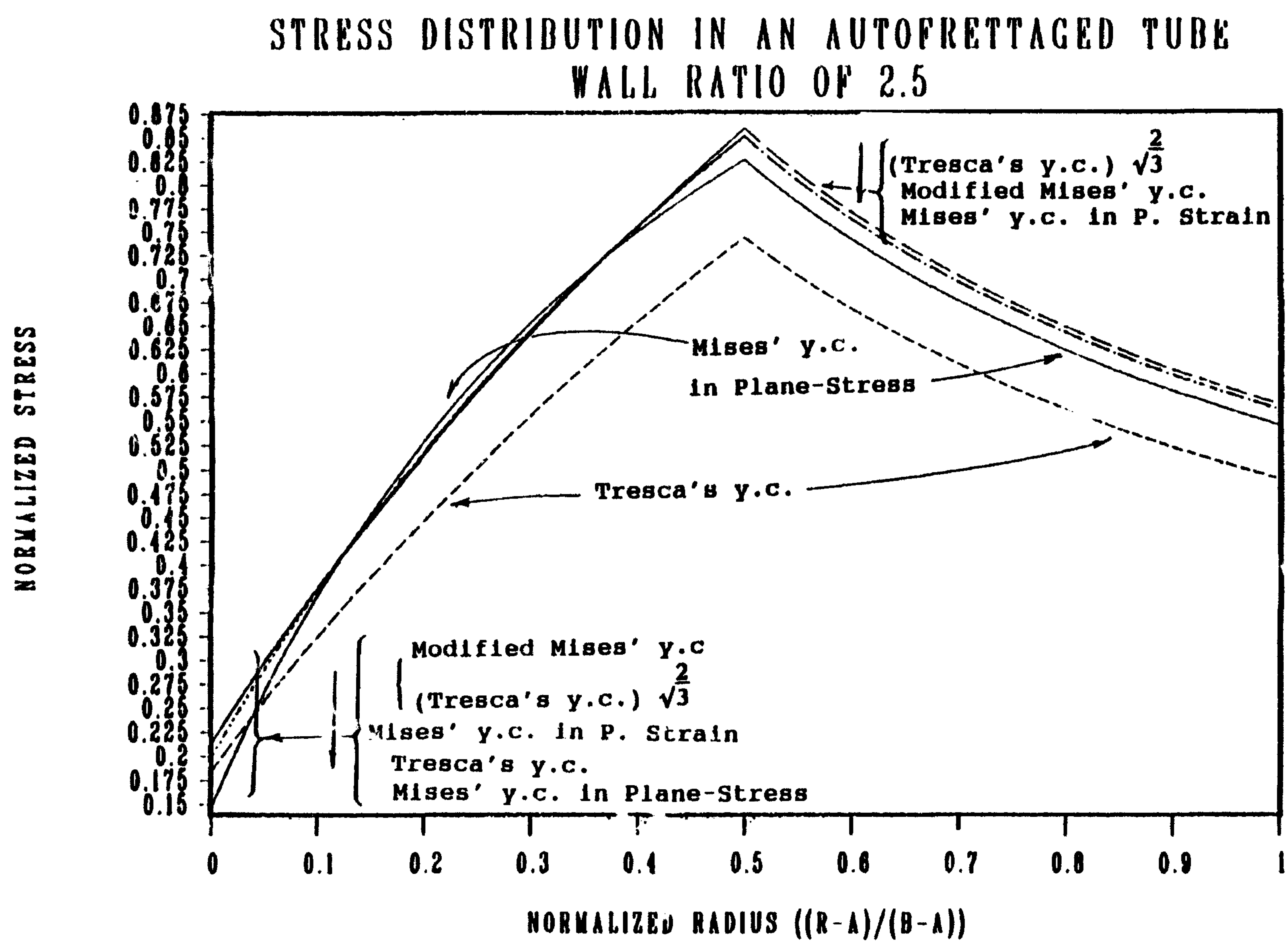

Figure 11a. **Tangential stress component:** Stress distribution in an autofrettaged pressure vessel with a wall ratio of $b/a = 2.5$ under (autofrettaging) pressure of 50 percent autofrettage.

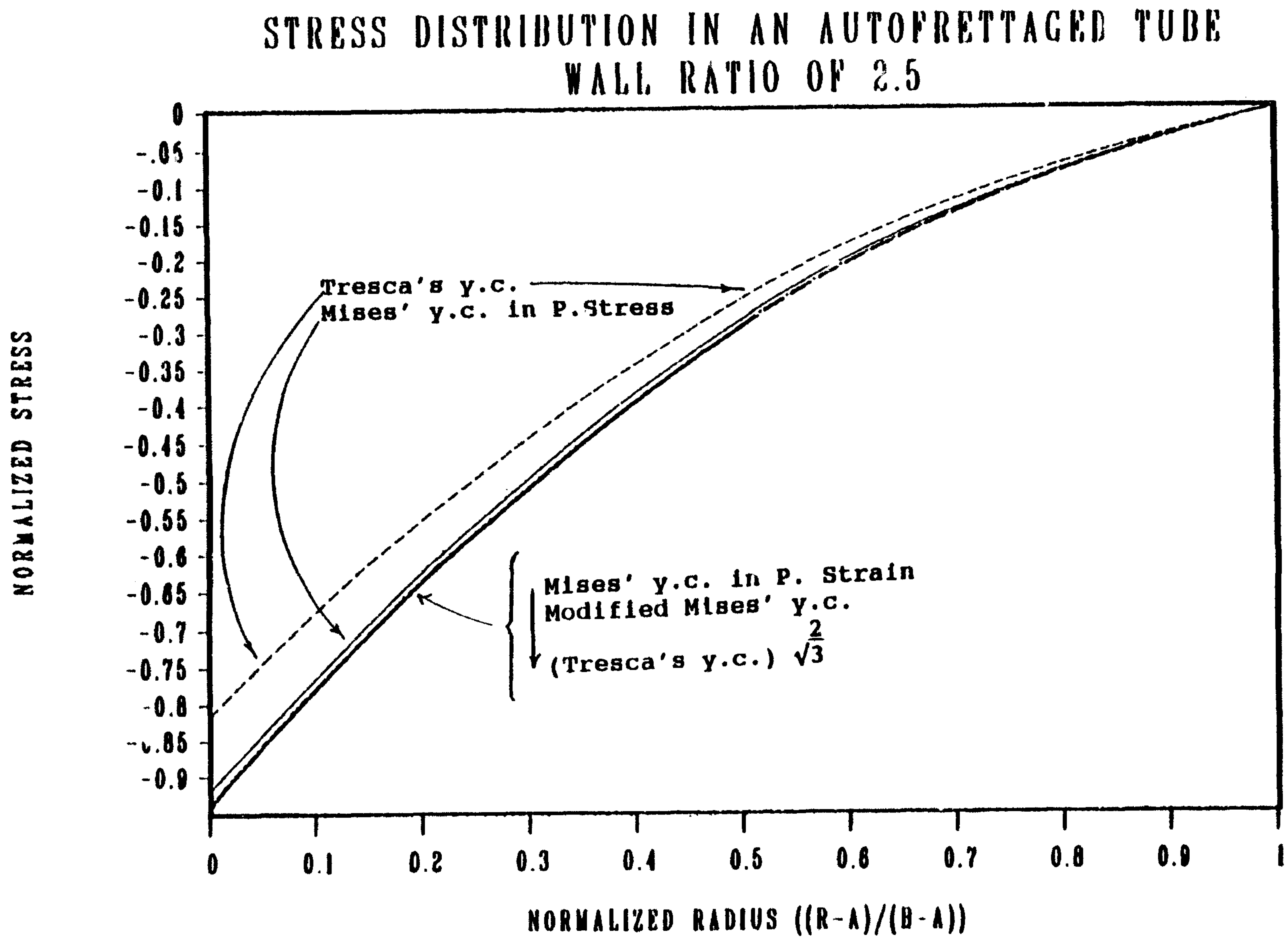

Figure 11b. **Radial stress component:** Stress distribution in an autofrettaged pressure vessel with a wall ratio of b/a = 2.5 under (autofrettaging) pressure of 50 percent autofrettage.

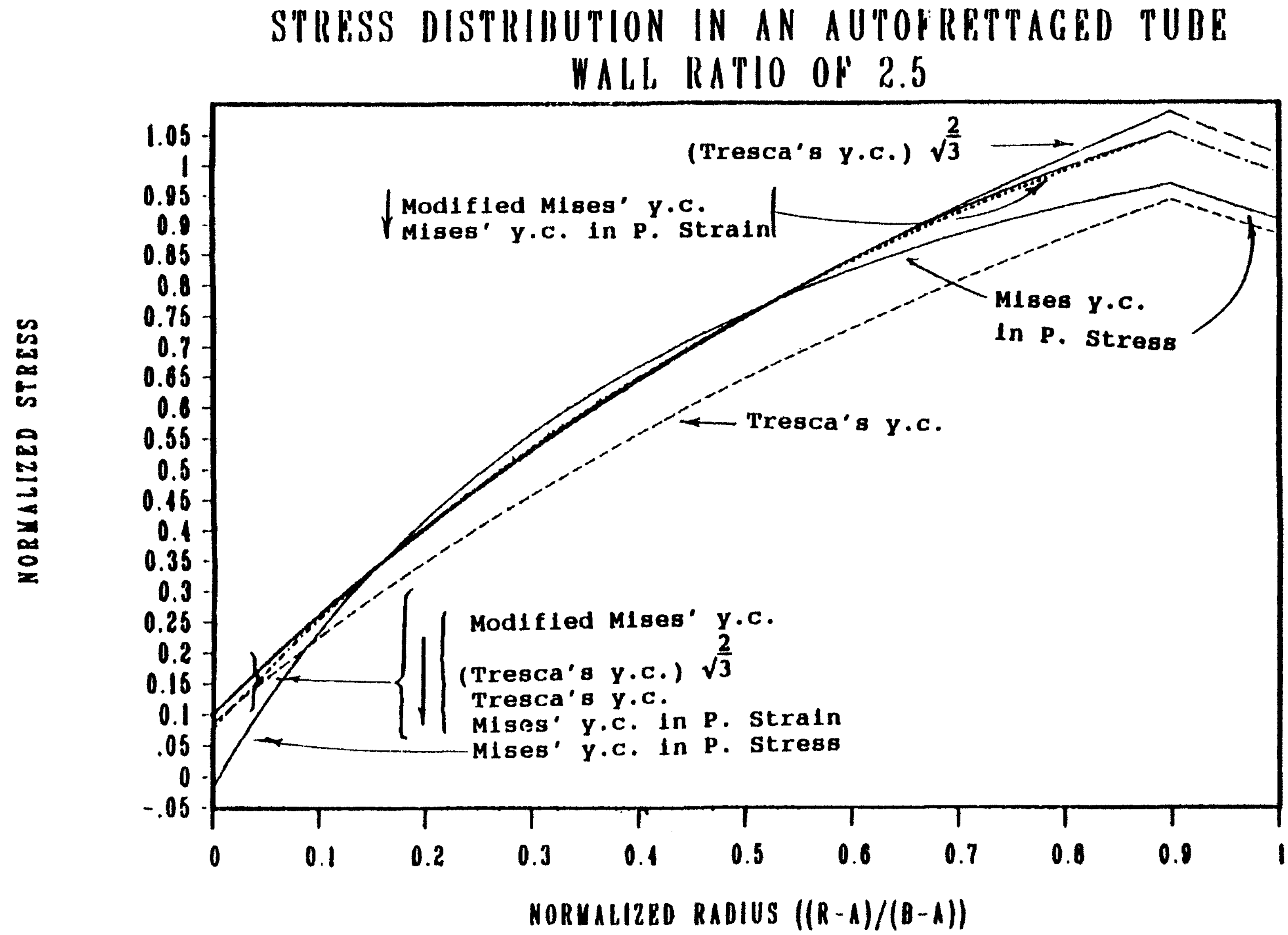

Figure 12a. **Tangential stress component**: Stress distribution in an autofrettaged pressure vessel with a wall ratio of b/a = 2.5 under (autofrettaging) pressure of 90 percent autofrettage.

STRESS DISTRIBUTION IN AN AUTOFRETTAGED TUBE WALL RATIO OF 2.5

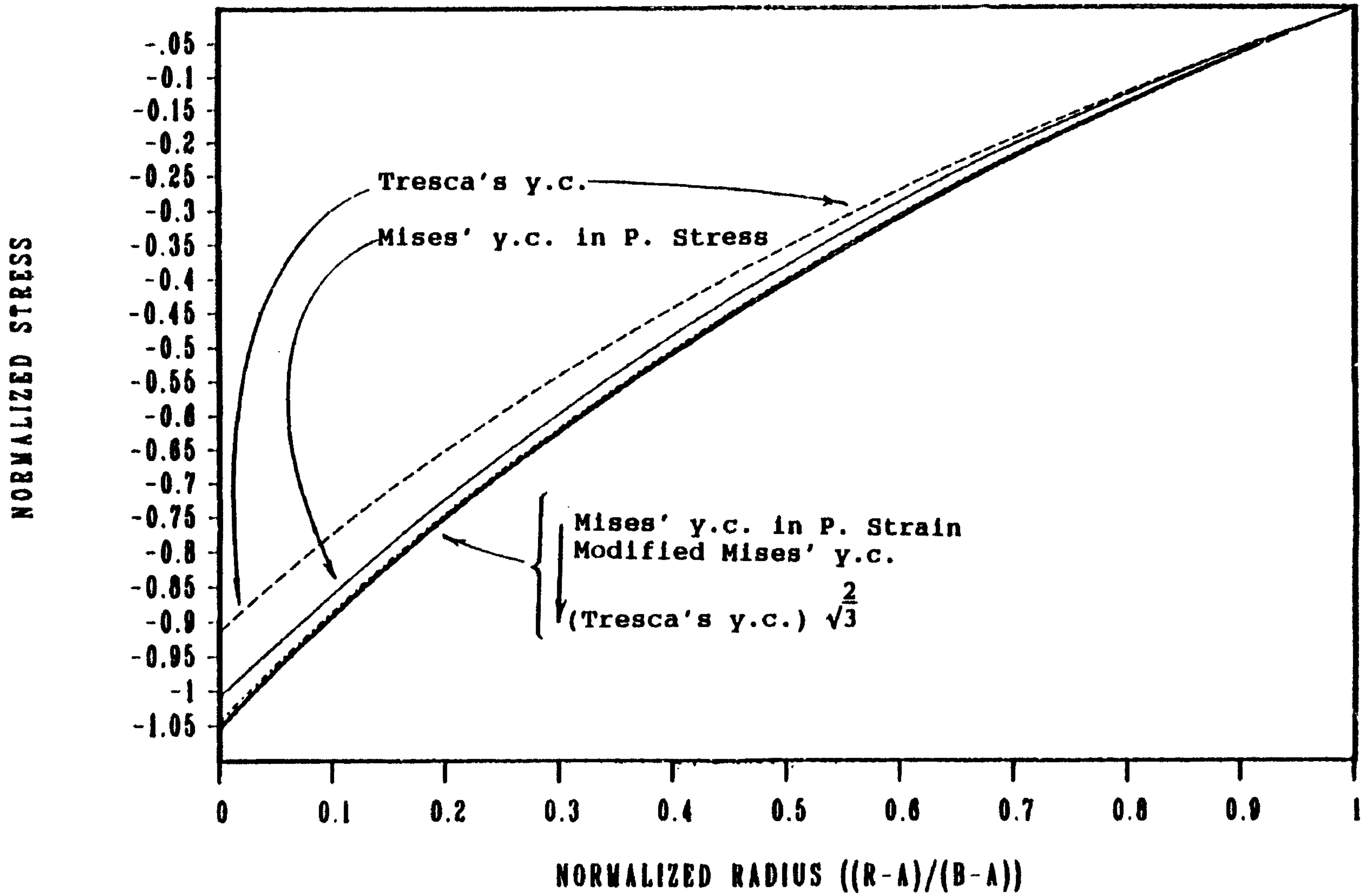

Figure 12b. **Radial stress component**: Stress distribution in an autofrettaged pressure vessel with a wall ratio of b/a = 2.5 under (autofrettaging) pressure of 90 percent autofrettage.

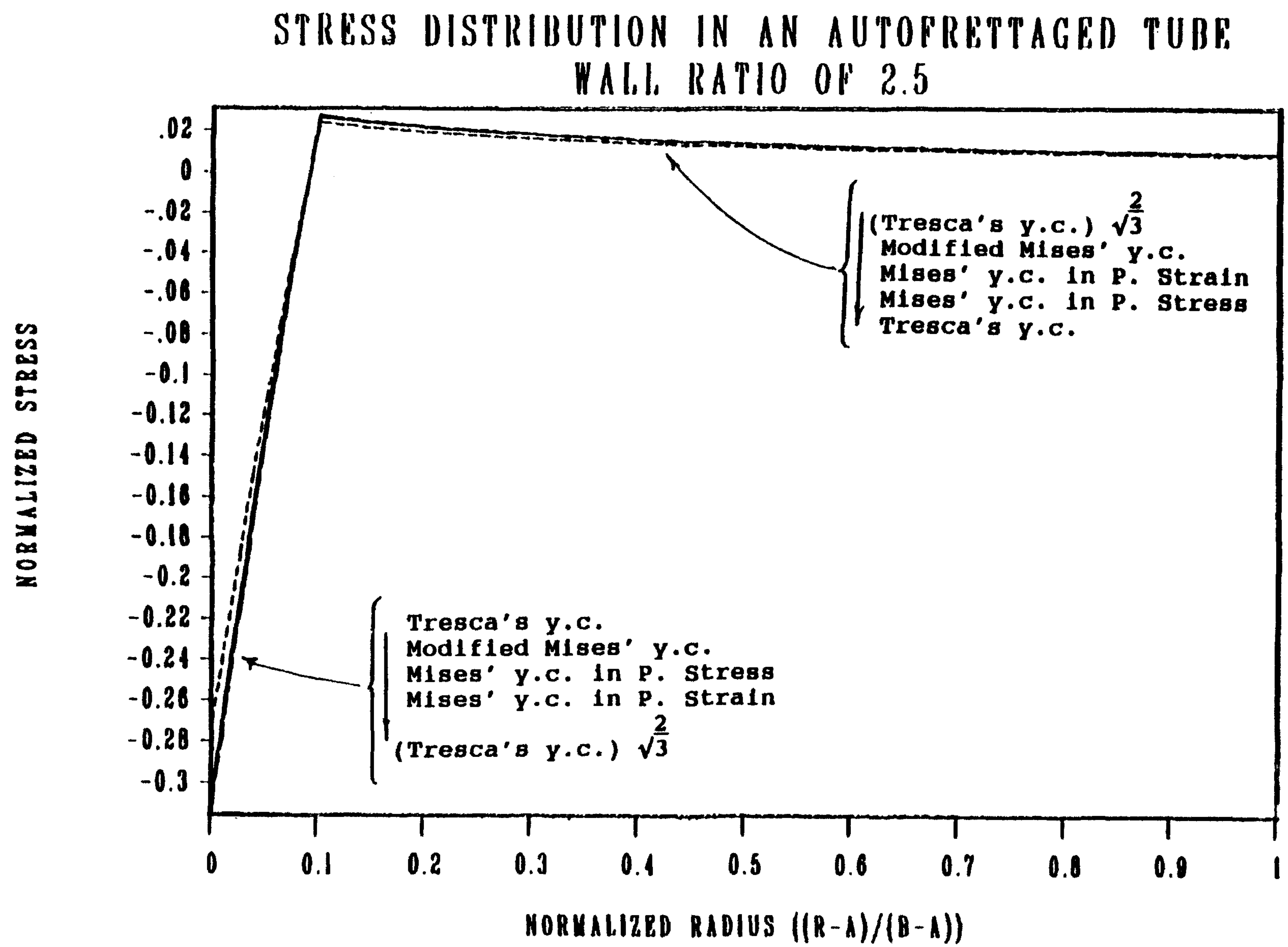

Figure 13a. **Tangential stress component:** Stress distribution in an autofrettaged pressure vessel with a wall ratio of b/a = 2.5 after depressurization of 10 percent autofrettage.

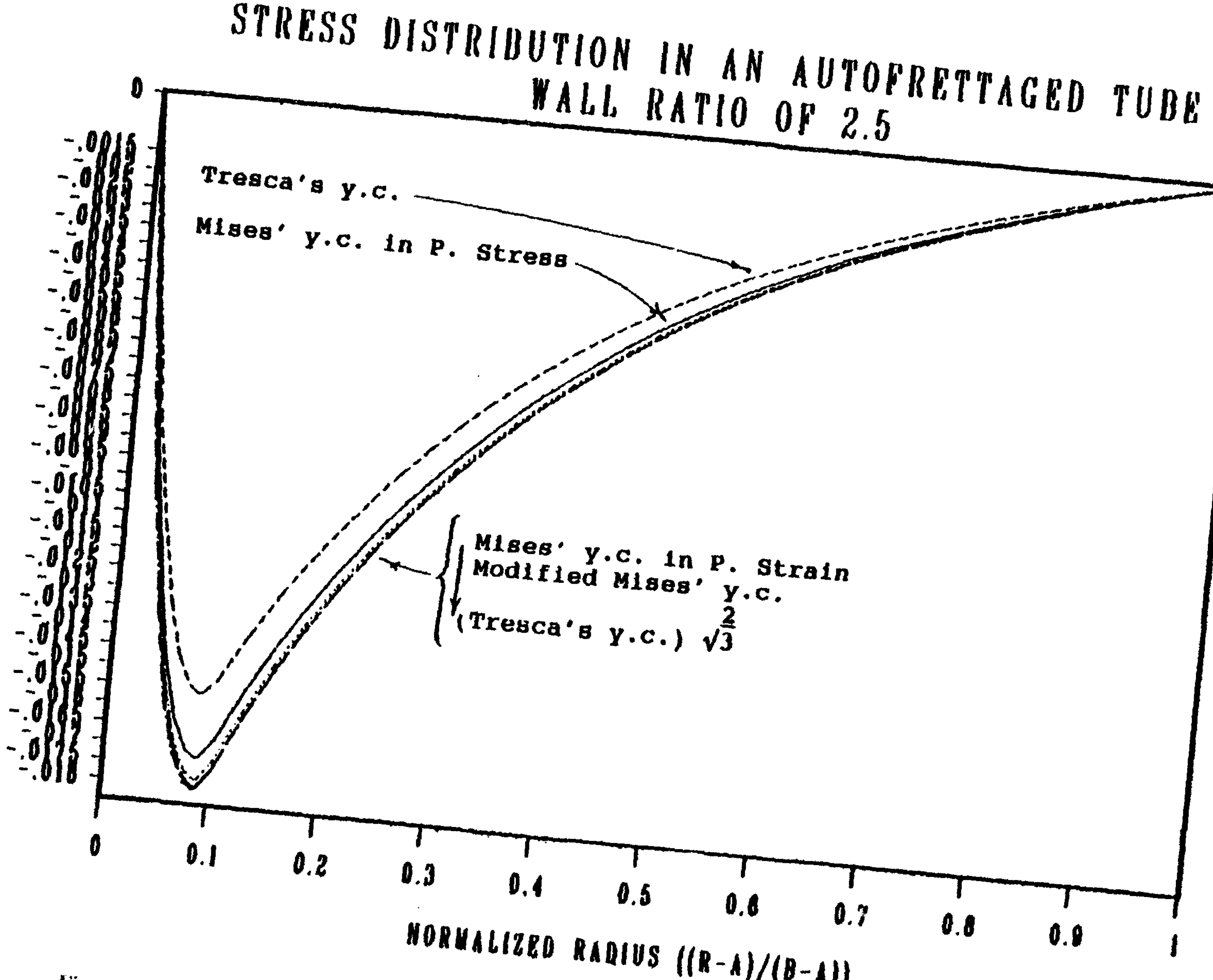

Figure 13b. **Radial stress component**: Stress distribution in an autofrettaged pressure vessel with a wall ratio of b/a = 2.5 after depressurization of 10 percent autofrettage.

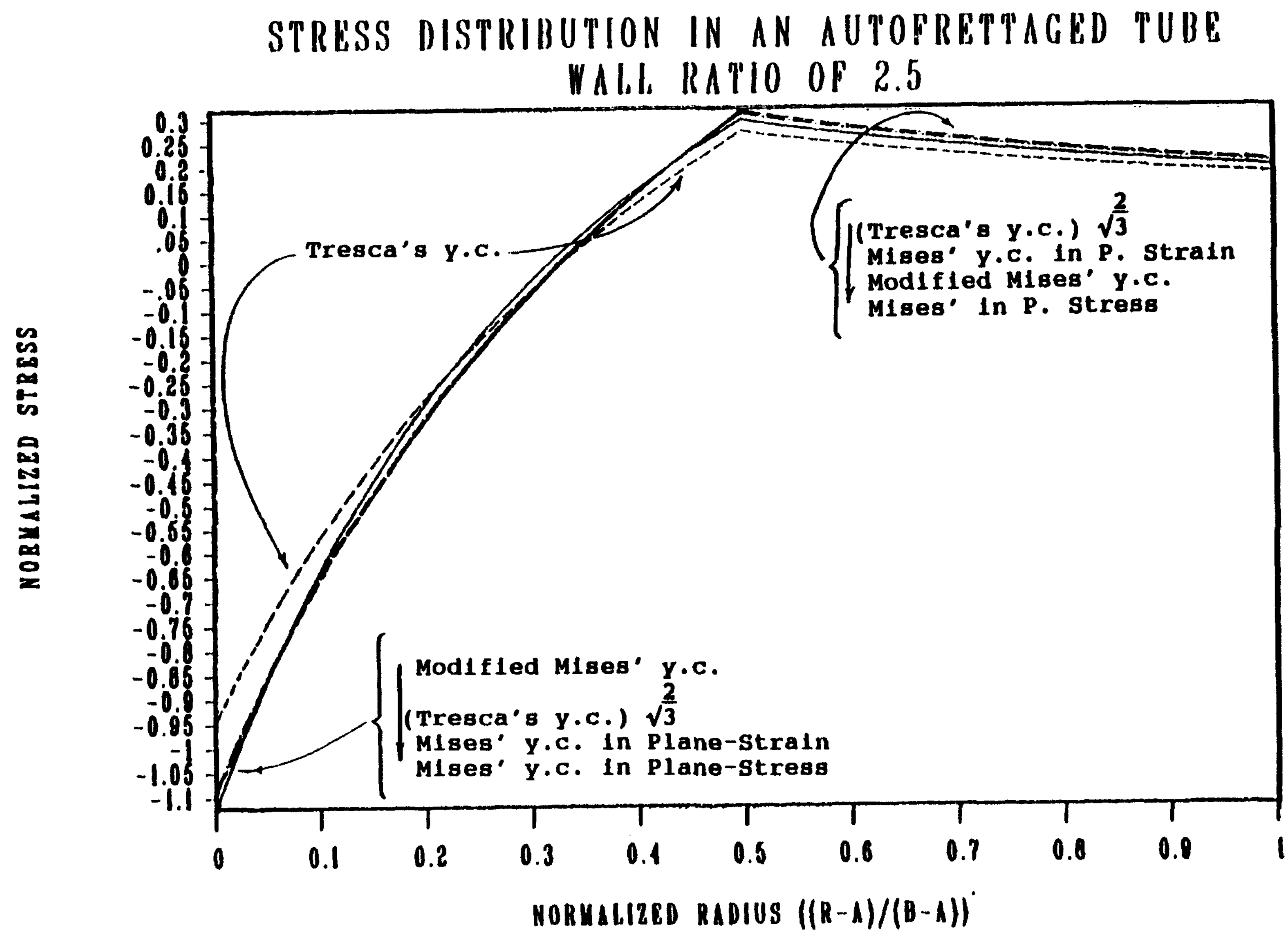

Figure 14a. **Tangential stress component:** Stress distribution in an autofrettaged pressure vessel with a wall ratio of b/a = 2.5 after depressurization of 50 percent autofrettage.

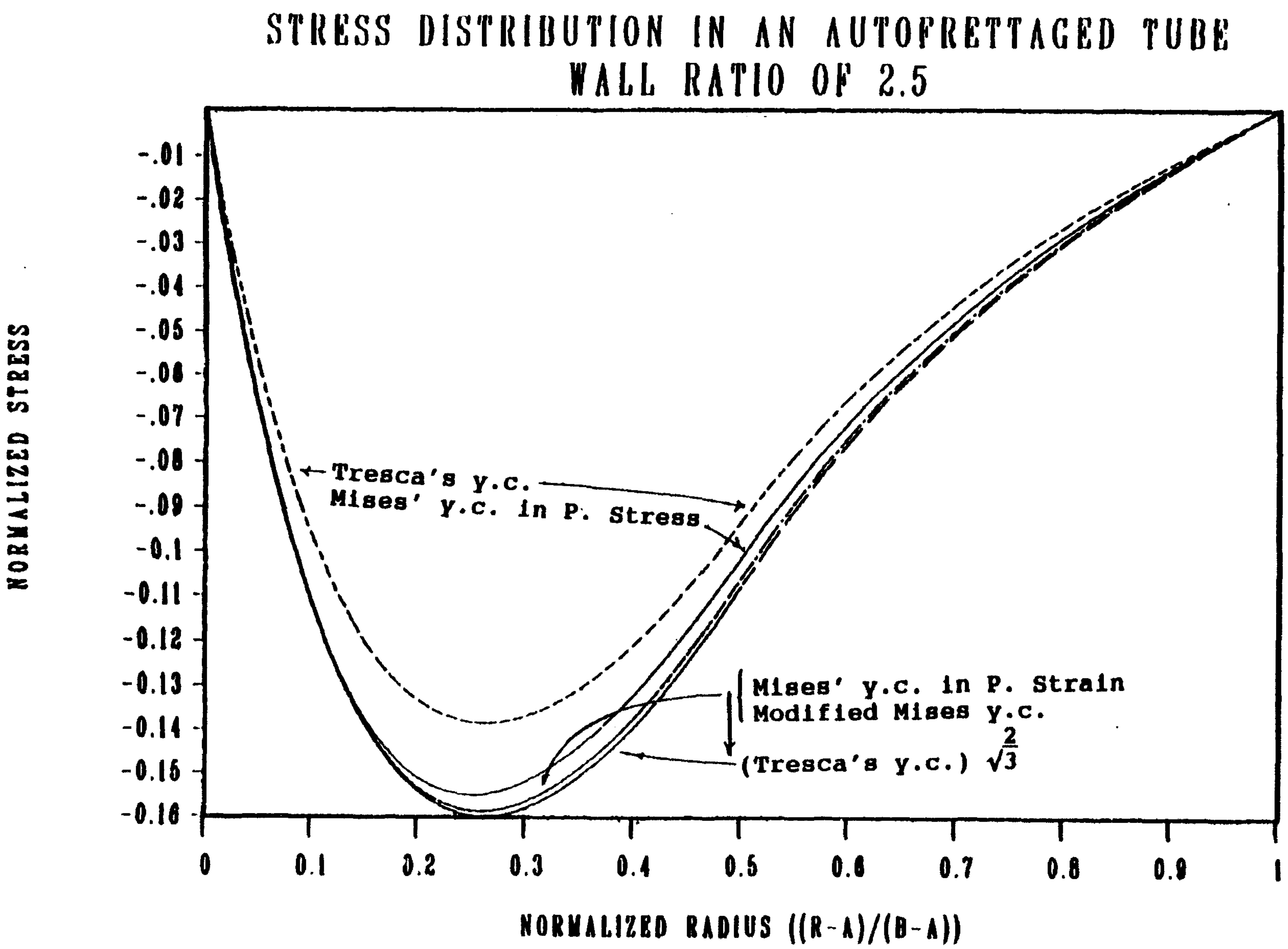

Figure 14b. **Radial stress component:** Stress distribution in an autofrettaged pressure vessel with a wall ratio of b/a = 2.5 after depressurization of 50 percent autofrettage.

STRESS DISTRIBUTION IN AN AUTOFRETTAGED TUBE WALL RATIO OF 2.5

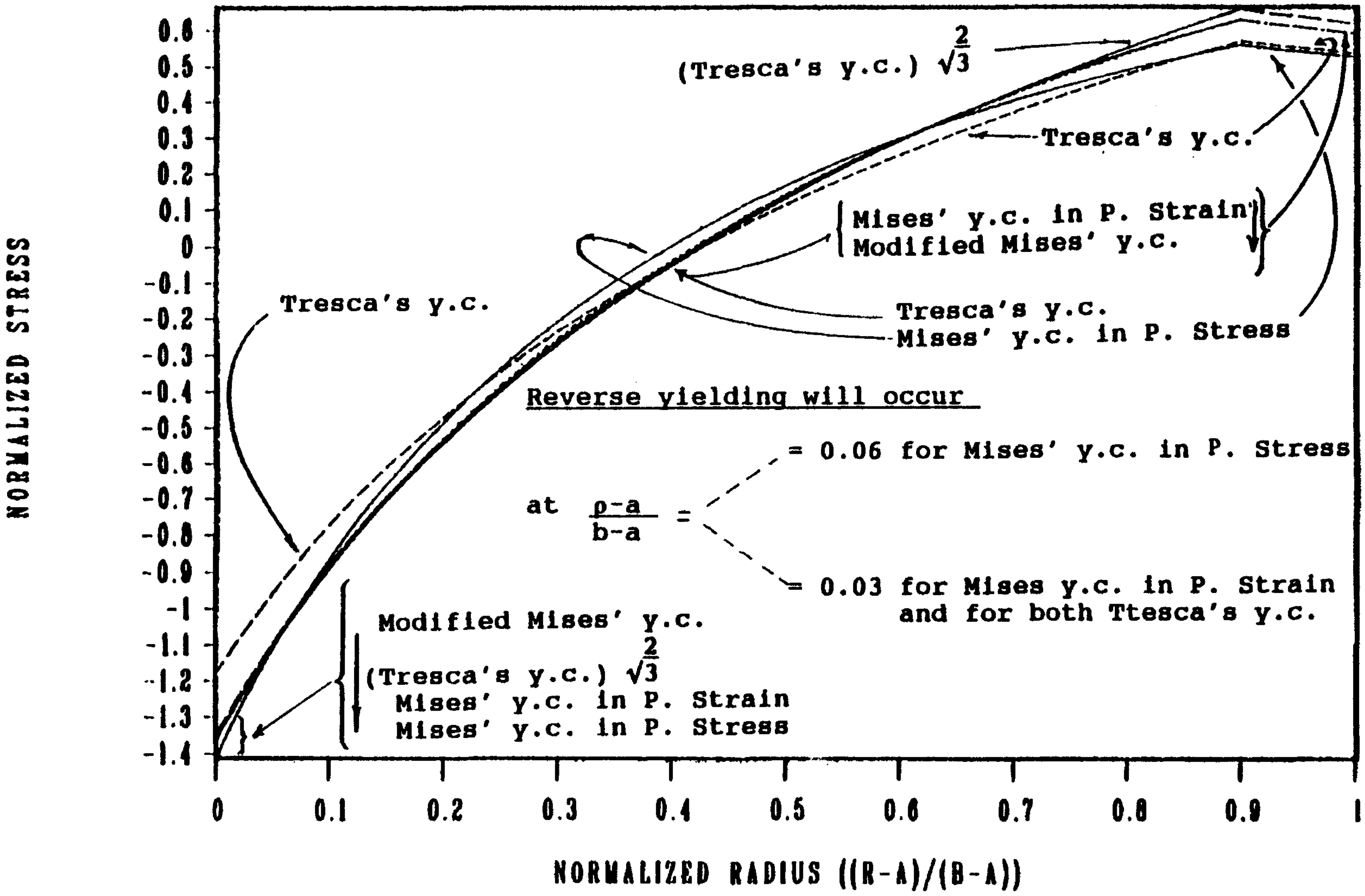

Figure 15a. **Tangential stress component**: Stress distribution in an autofrettaged pressure vessel with a wall ratio of b/a = 2.5 after depressurization of 90 percent autofrettage.

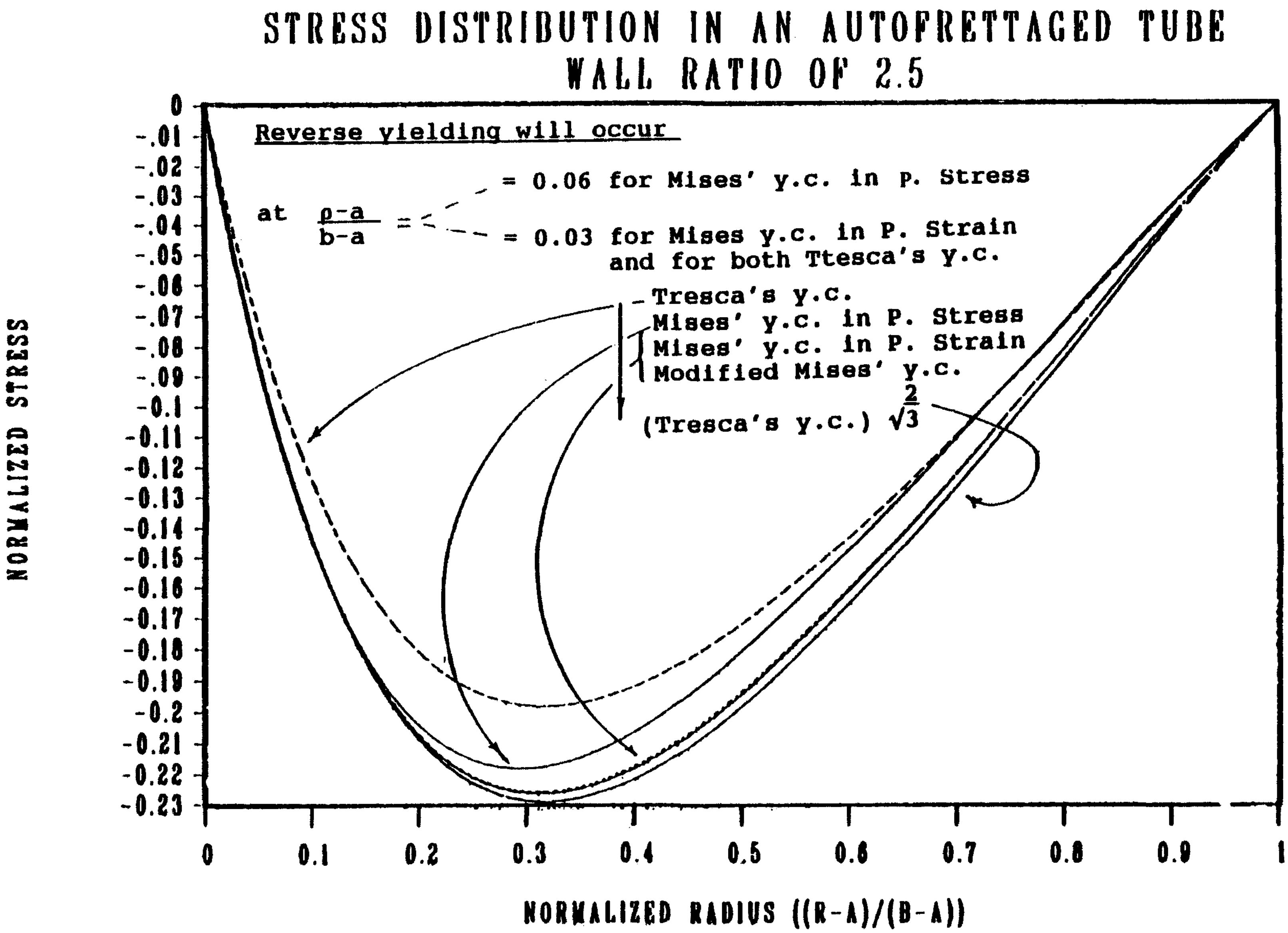

Figure 15b. **Radial stress component**: Stress distribution in an autofrettaged pressure vessel with a wall ratio of b/a = 2.5 after depressurization of 90 percent autofrettage.

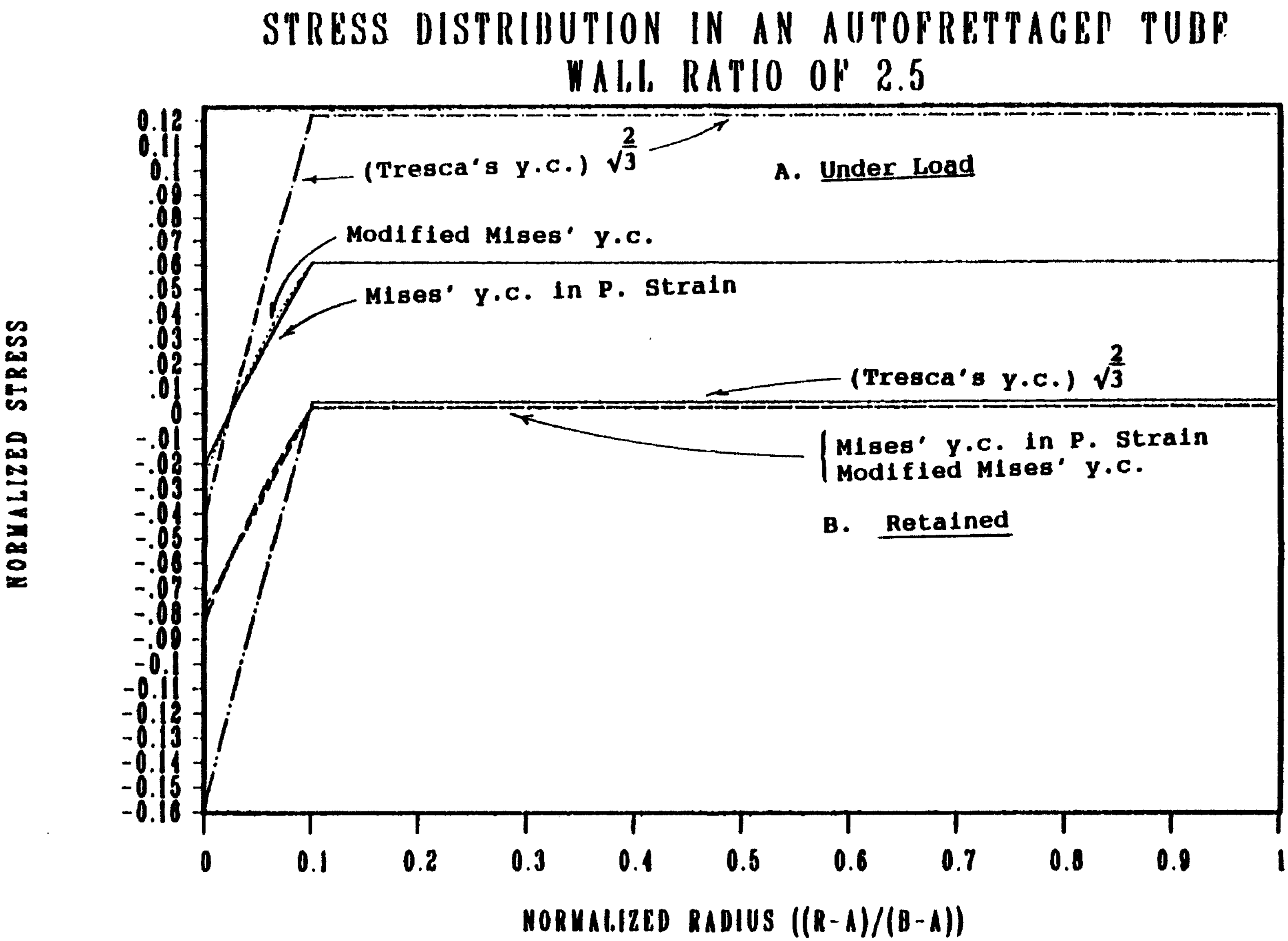

Figure 16. **Axial stress component:** Stress distribution in an autofrettaged pressure vessel with a wall ratio of b/a = 2.5 under (autofrettaging) pressure and after depressurization of 10 percent autofrettage.

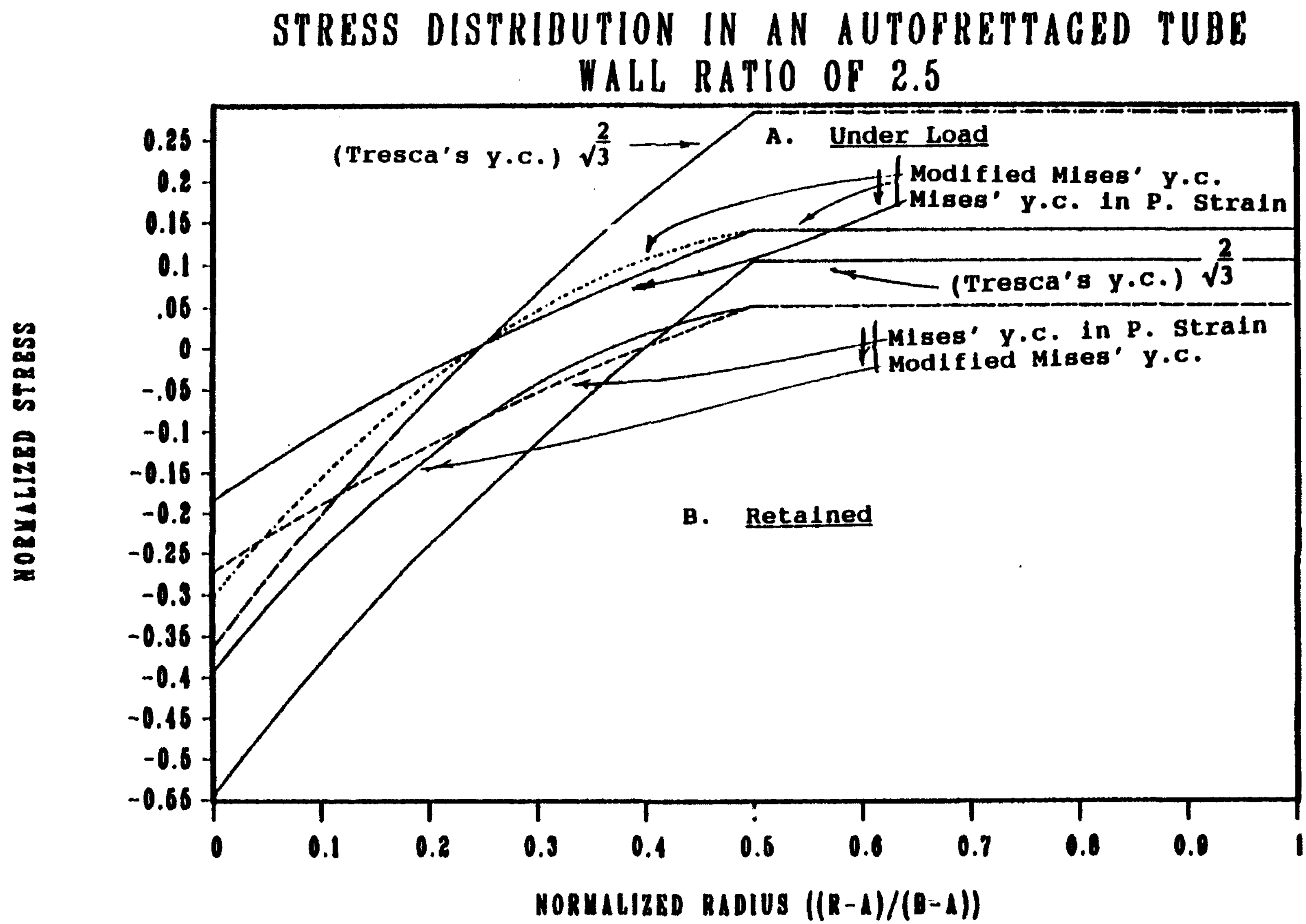

Figure 17. **Axial stress component:** Stress distribution in an autofrettaged pressure vessel with a wall ratio of b/a = 2.5 under (autofrettaging) pressure and after depressurization of 50 percent autofrettage.

STRESS DISTRIBUTION IN AN AUTOFRETTAGED TUBE WALL RATIO OF 2.5

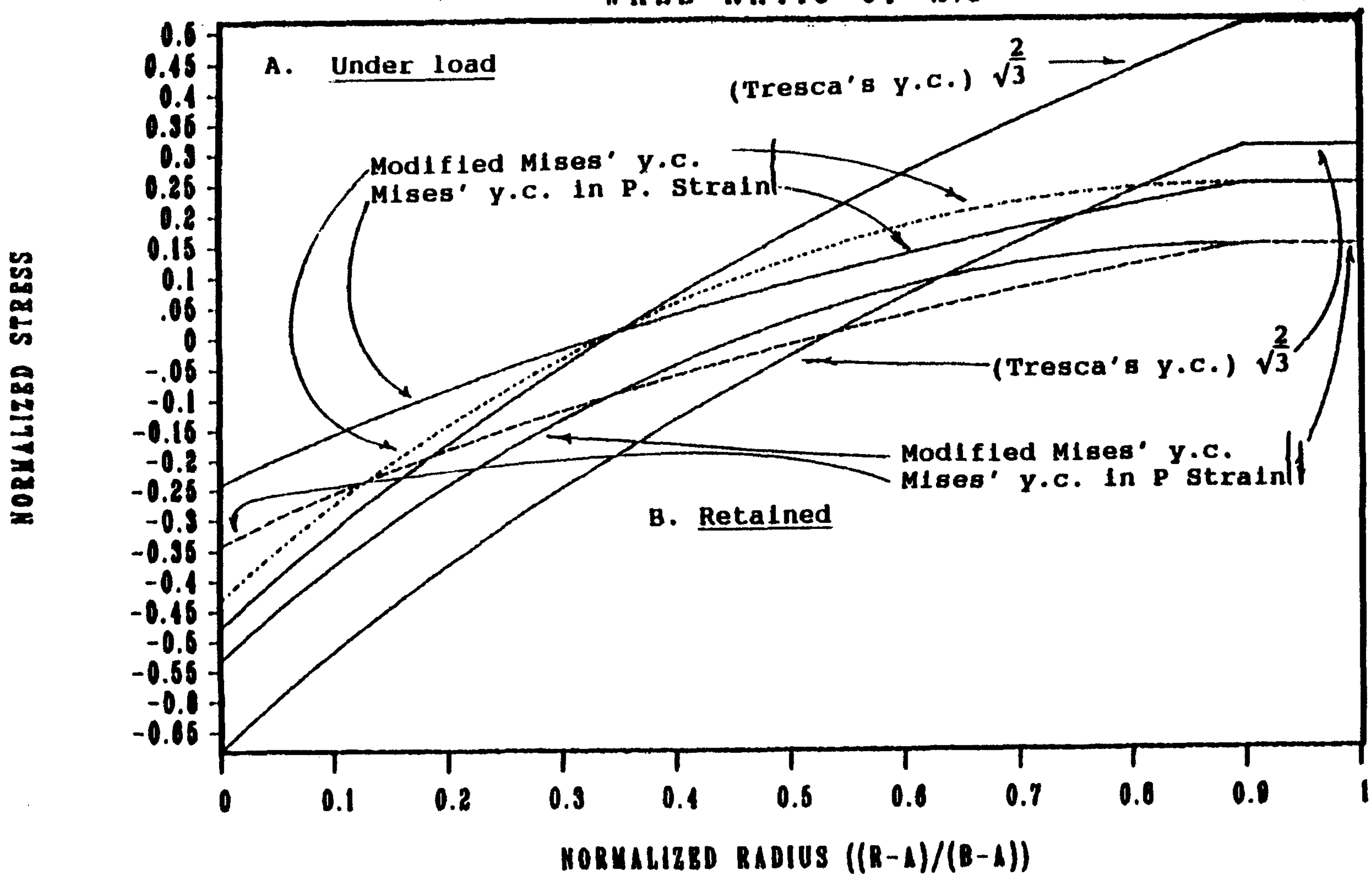

Figure 18. **Axial stress component:** Stress distribution in an autofrettaged pressure vessel with a wall ratio of b/a = 2.5 under (autofrettaging) pressure and after depressurization of 90 percent autofrettage.

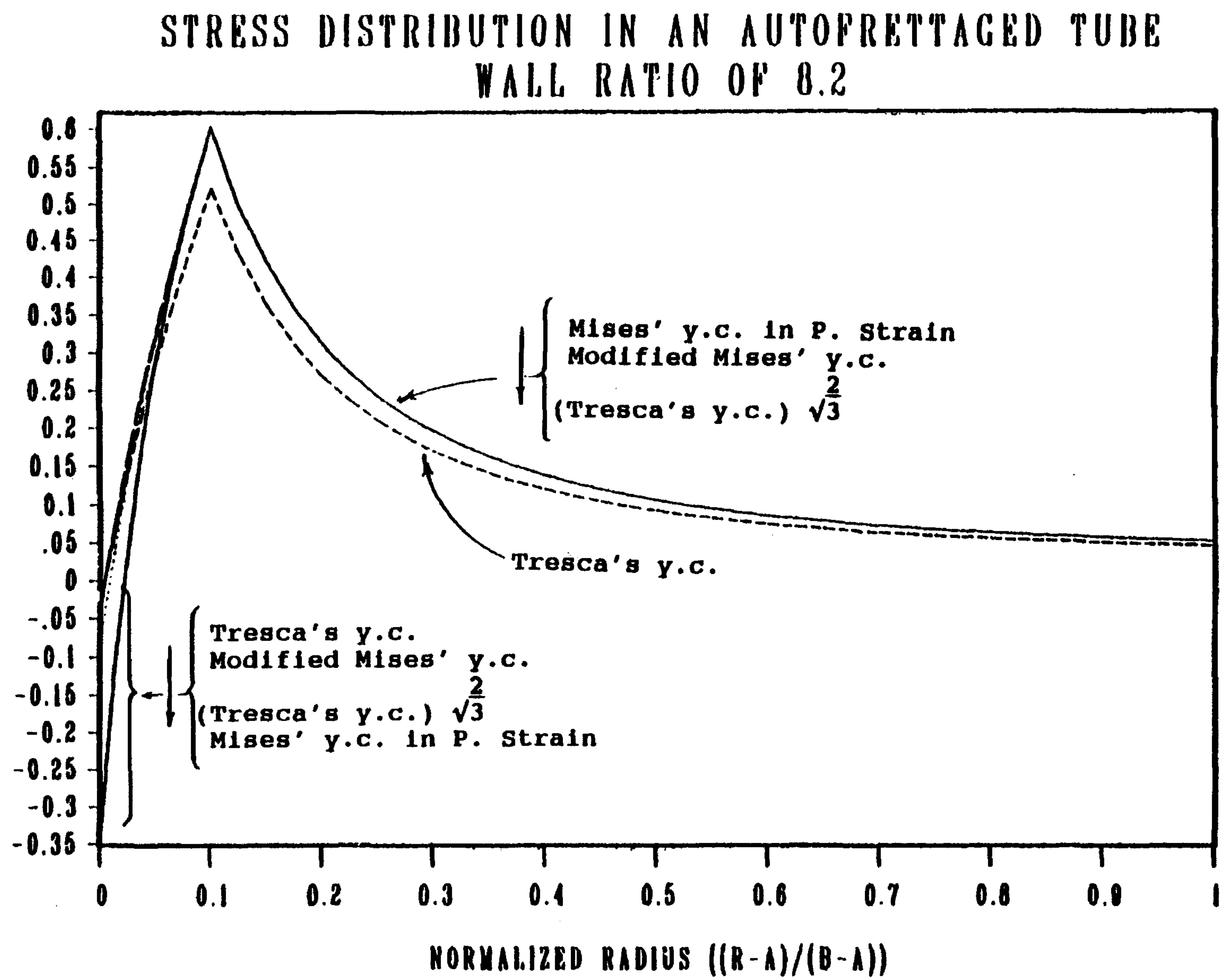

Figure 19a. **Tangential stress component:** Stress distribution in an autofrettaged pressure vessel with a wall ratio of b/a = 8.2 under (autofrettaging) pressure of 10 percent autofrettage.

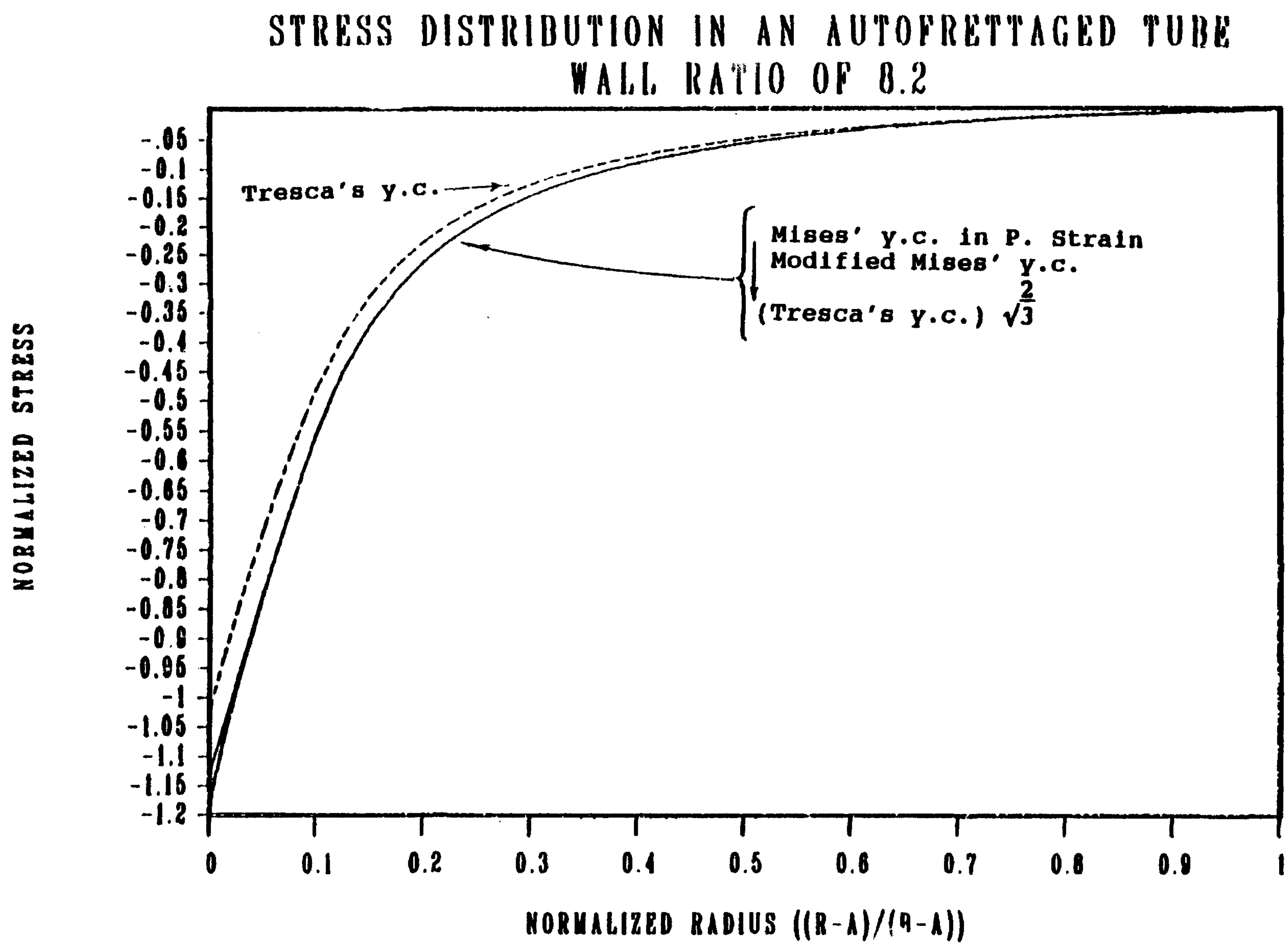

Figure 19b. **Radial stress component:** Stress distribution in an autofrettaged pressure vessel with a wall ratio of b/a = 8.2 under (autofrettaging) pressure of 10 percent autofrettage.

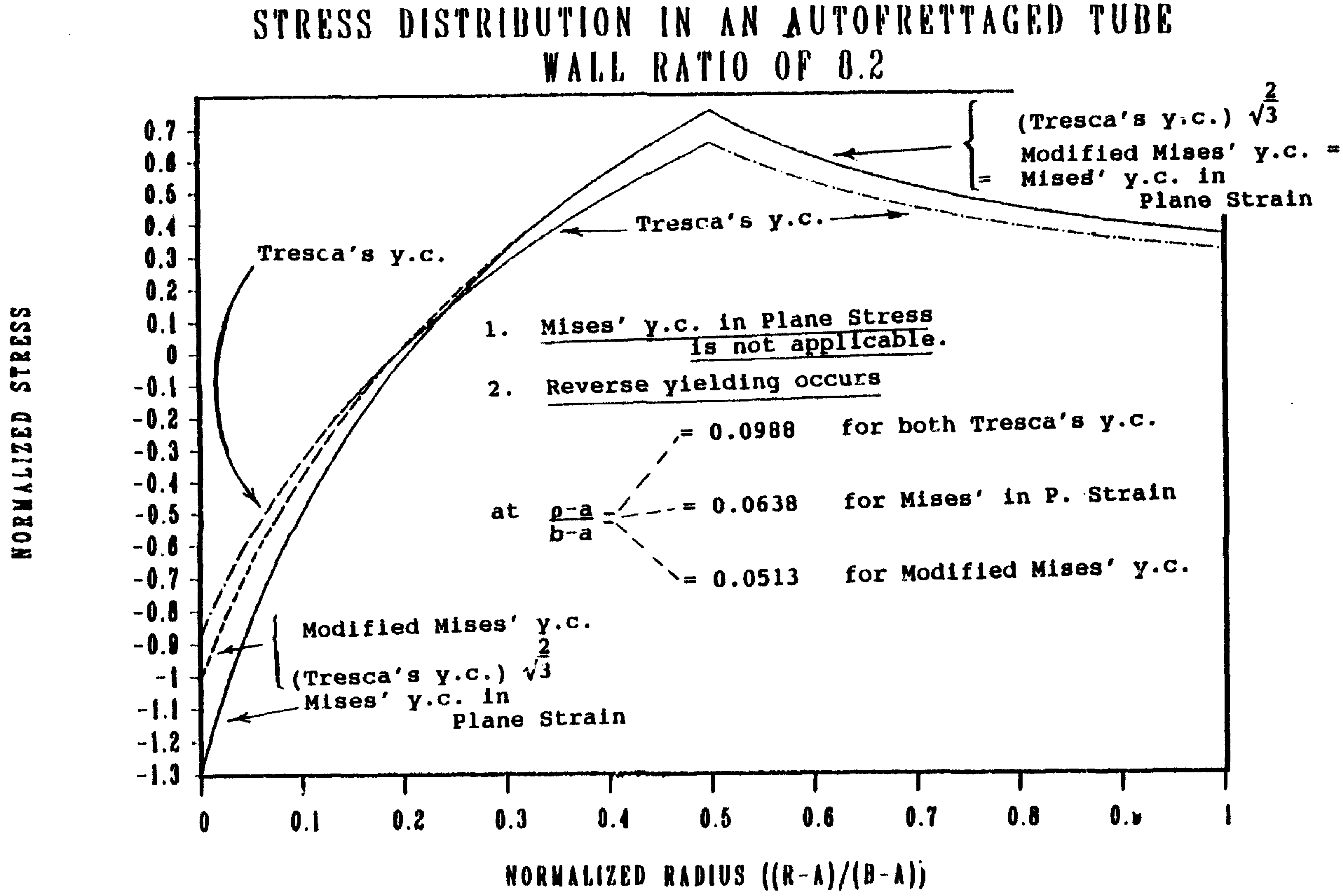

Figure 20a. **Tangential stress component:** Stress distribution in an autofrettaged pressure vessel with a wall ratio of b/a = 8.2 under (autofrettaging) pressure of 50 percent autofrettage.

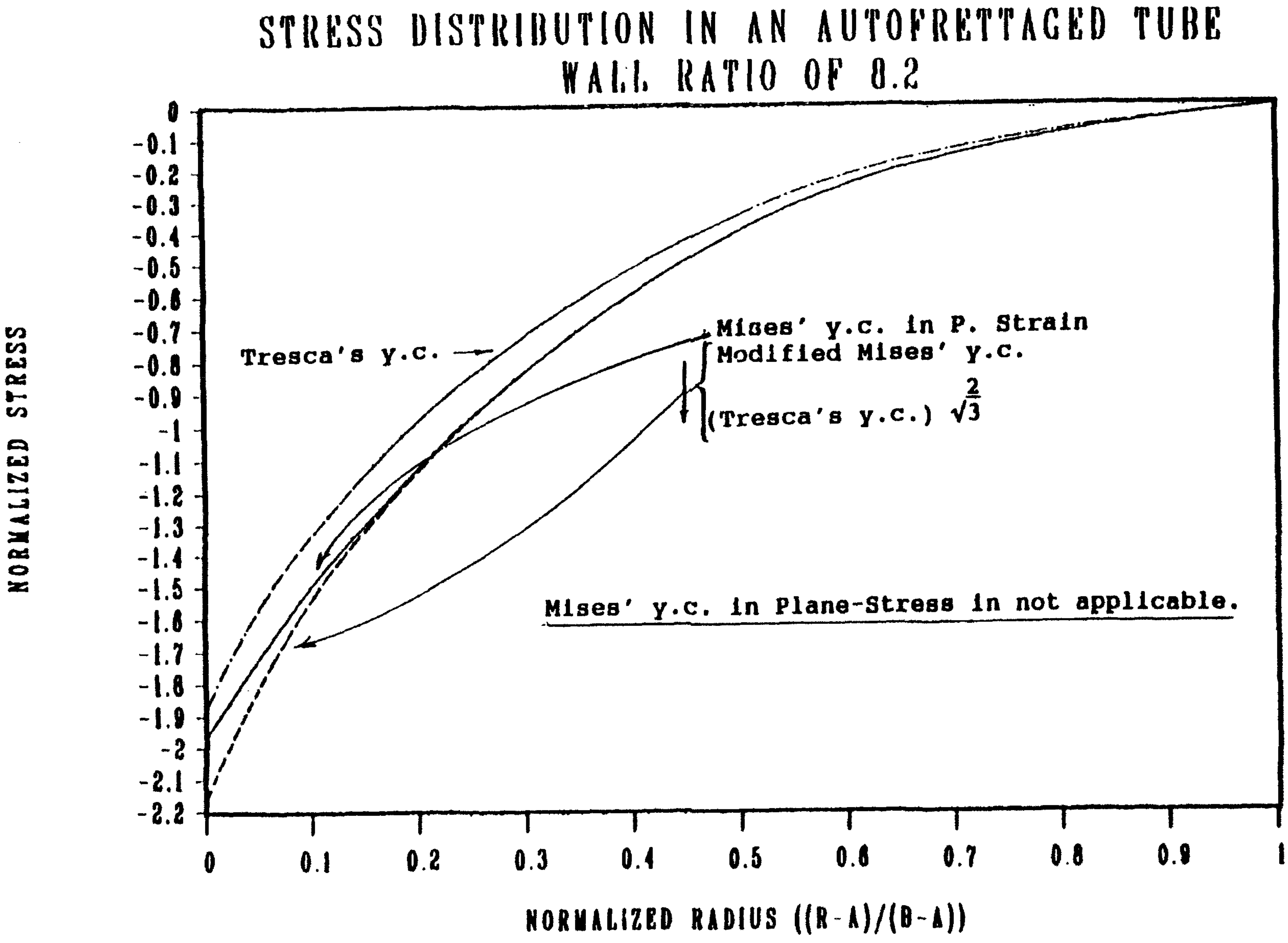

Figure 20b. **Radial stress component**: Stress distribution in an autofrettaged pressure vessel with a wall ratio of b/a = 8.2 under (autofrettaging) pressure of 50 percent autofrettage.

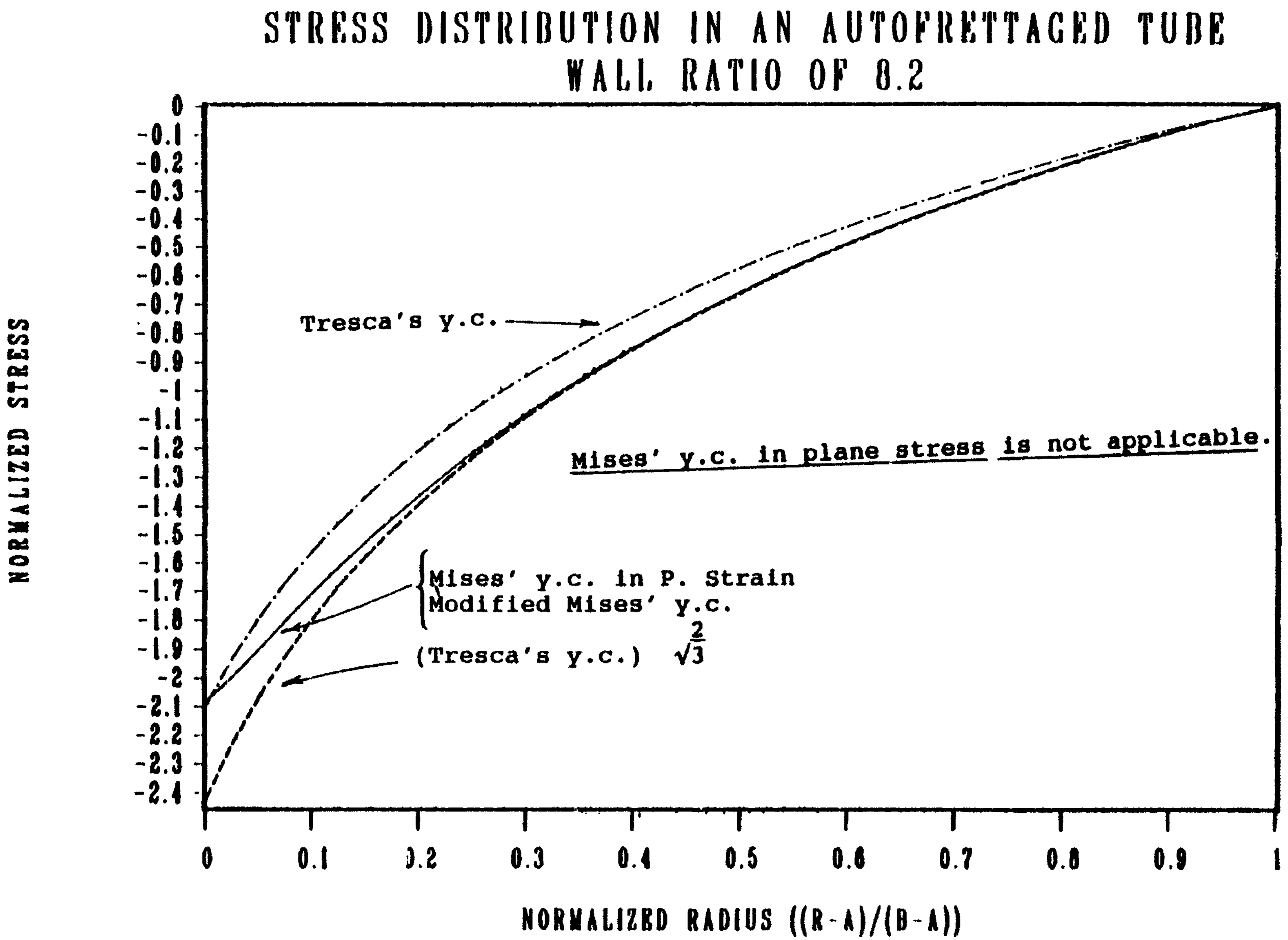

Figure 21b. **Radial stress component**: Stress distribution in an autofrettaged pressure vessel with a wall ratio of b/a = 8.2 under (autofrettaging) pressure of 90 percent autofrettage.

STRESS DISTRIBUTION IN AN AUTOFRETTAGED TUBE
WALL RATIO OF 8.2

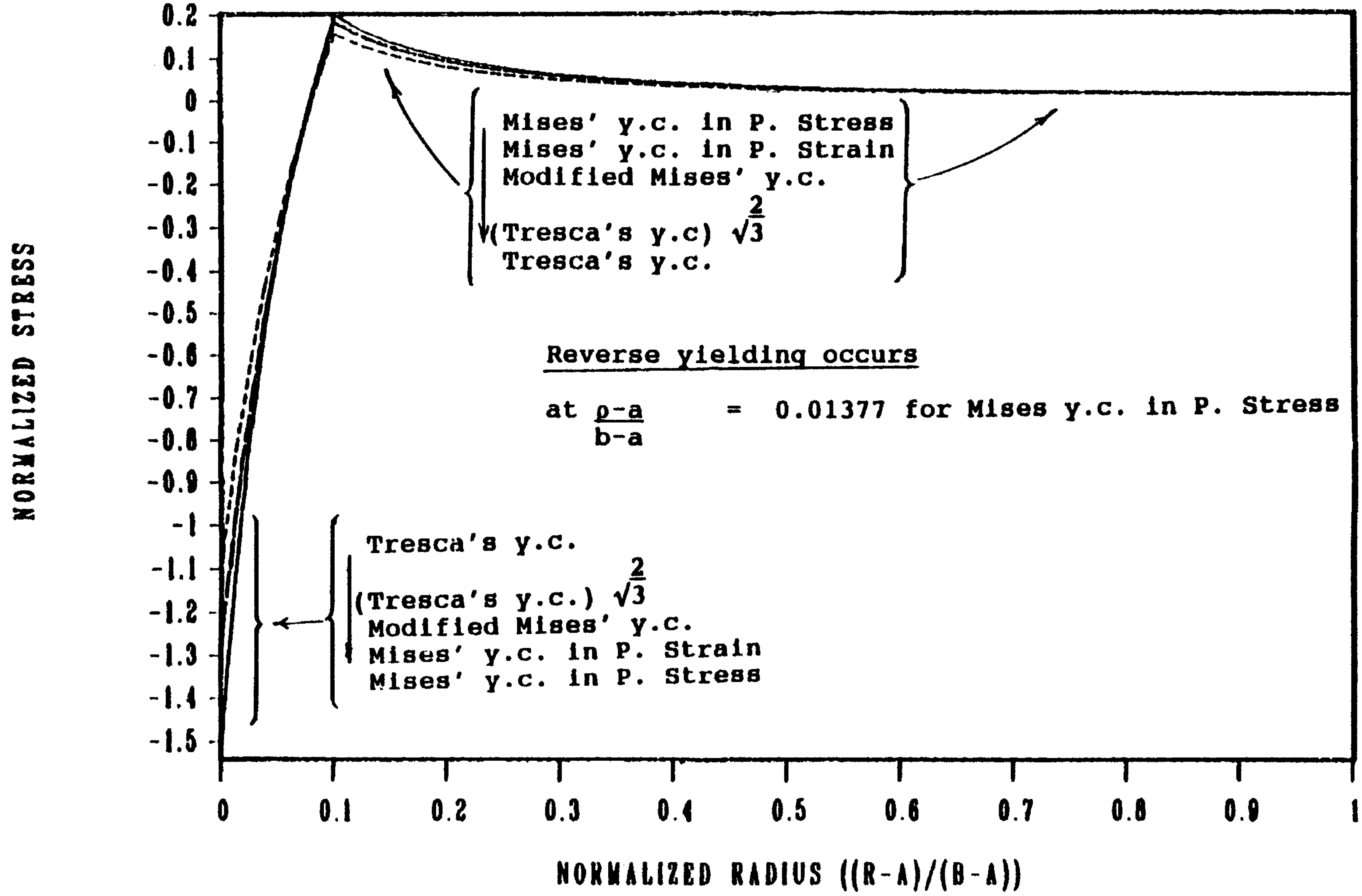

Figure 22a. **Tangential stress component**: Stress distribution in an autofrettaged pressure vessel with a wall ratio of b/a = 8.2 after depressurization of 10 percent autofrettage.

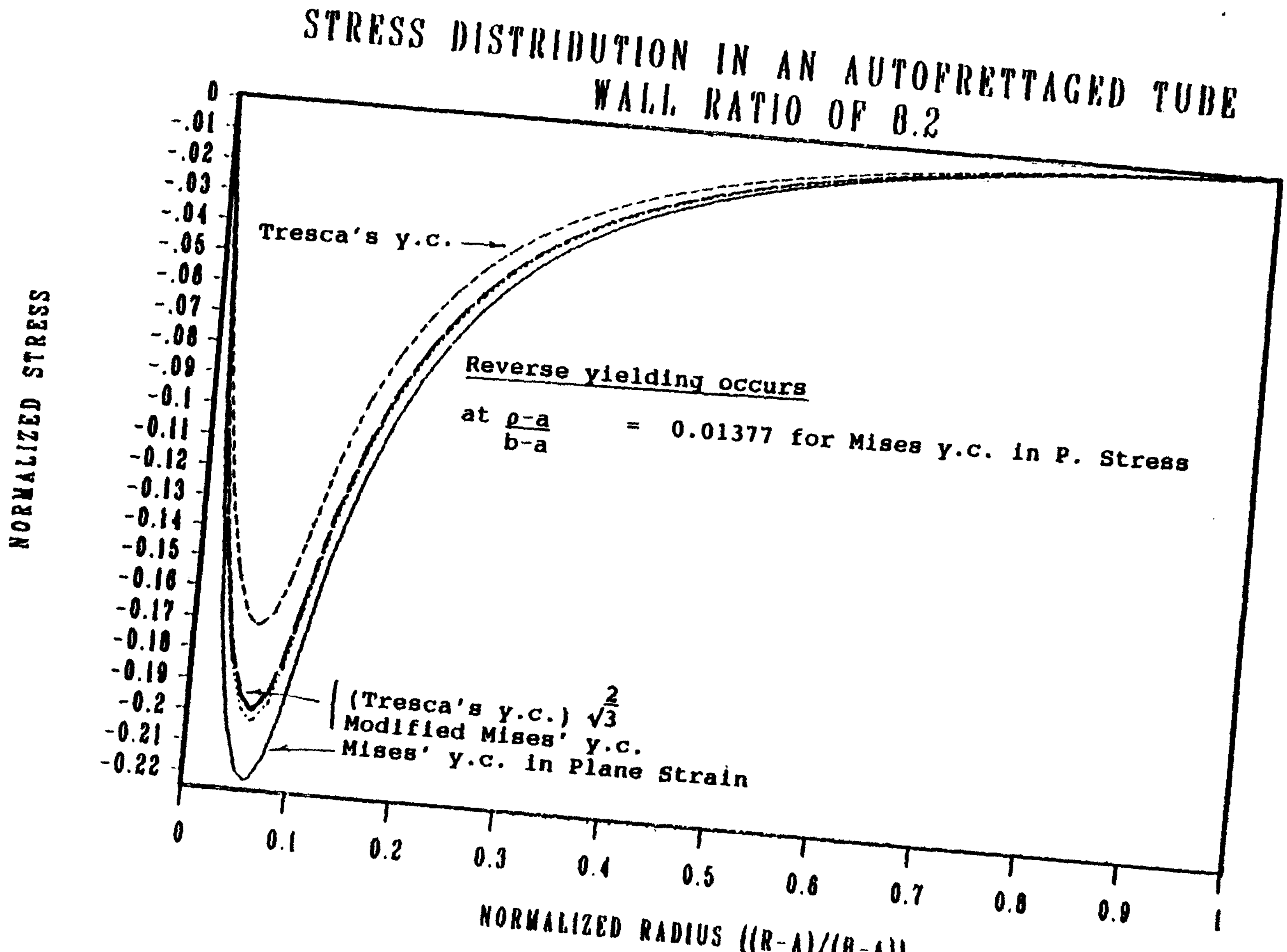

Figure 22b. **Radial stress component**: Stress distribution in an autofrettaged pressure vessel with a wall ratio of b/a = 8.2 after depressurization of 10 percent autofrettage.

STRESS DISTRIBUTION IN AN AUTOFRETTAGED TUBE WALL RATIO OF 8.2

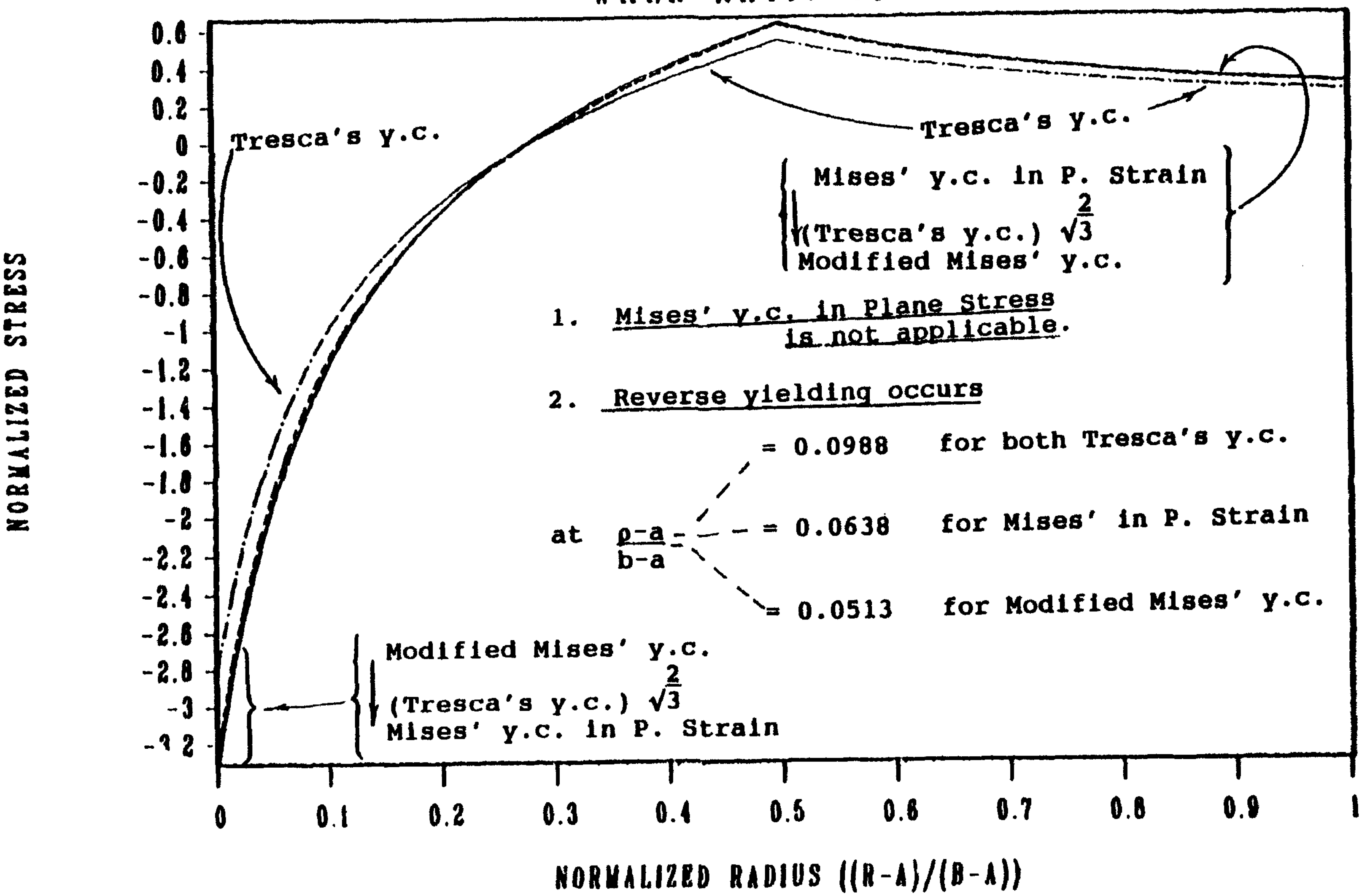

Figure 23a. **Tangential stress component:** Stress distribution in an autofrettaged pressure vessel with a wall ratio of b/a = 8.2 after depressurization of 50 percent autofrettage.

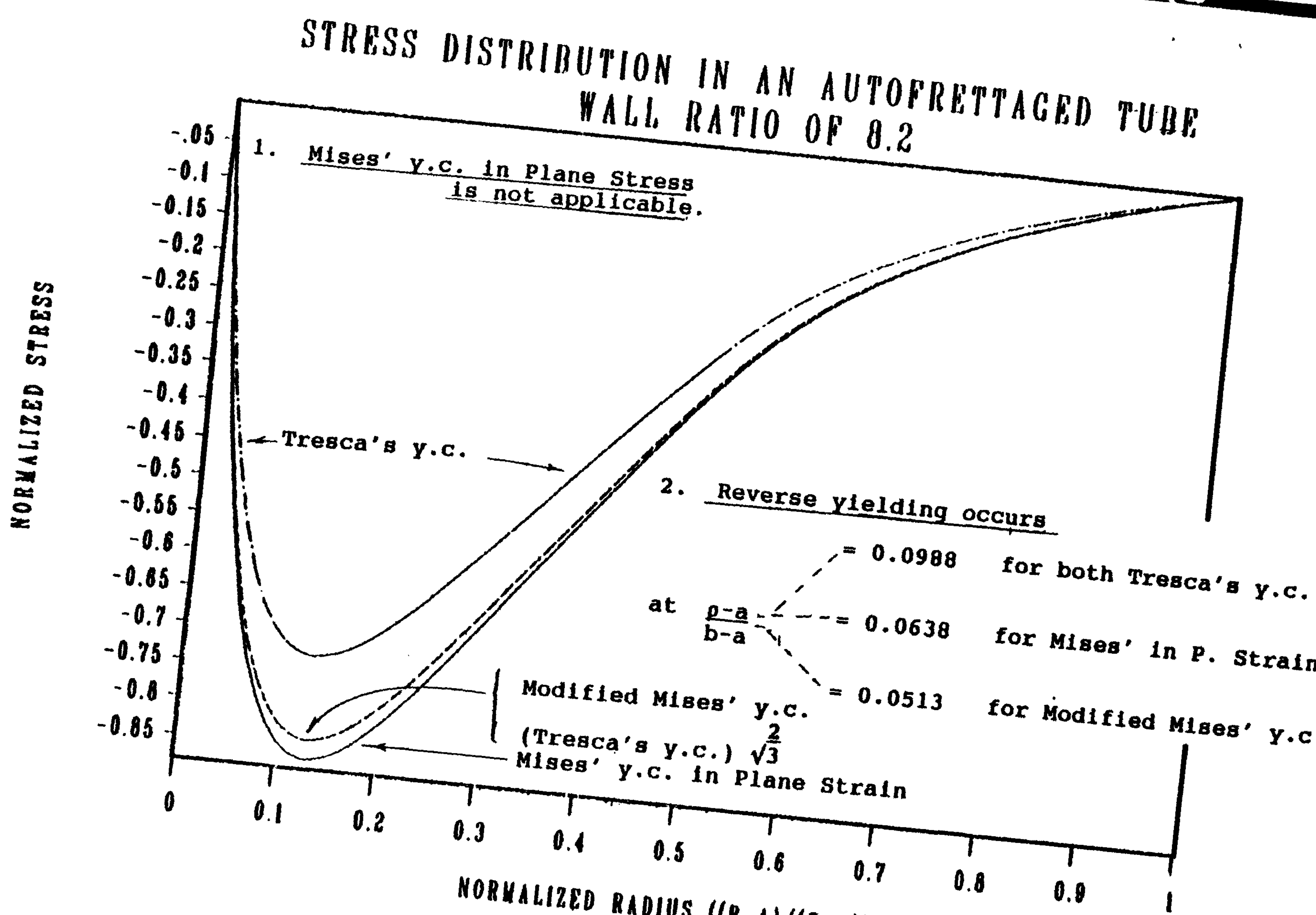

Figure 23b. **Radial stress component**: Stress distribution in an autofrettaged pressure vessel with a wall ratio of b/a = 8.2 after depressurization of 50 percent autofrettage.

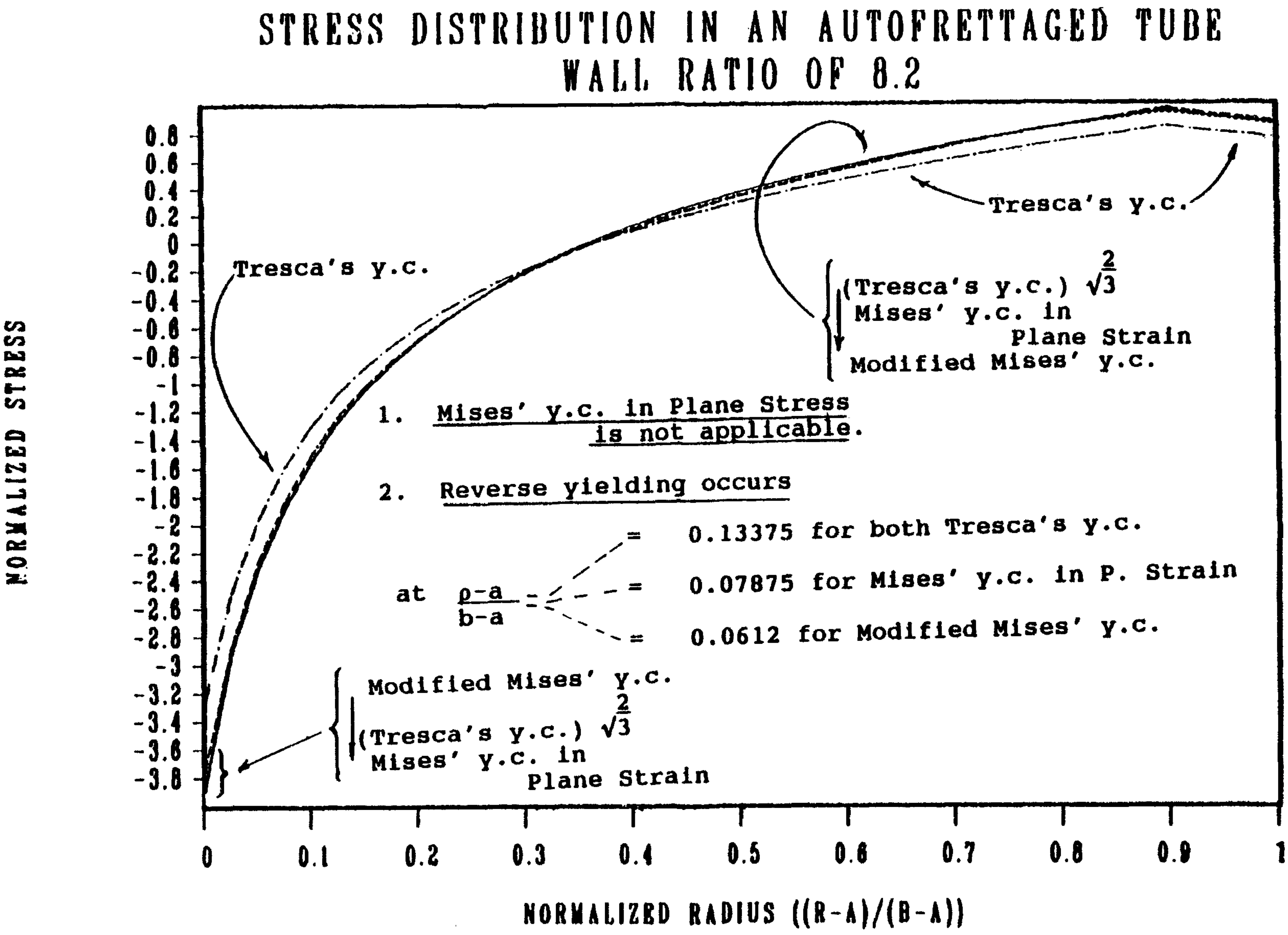

Figure 24a. **Tangential stress component**: Stress distribution in an autofrettaged pressure vessel with a wall ratio of b/a = 8.2 after depressurization of 90 percent autofrettage.

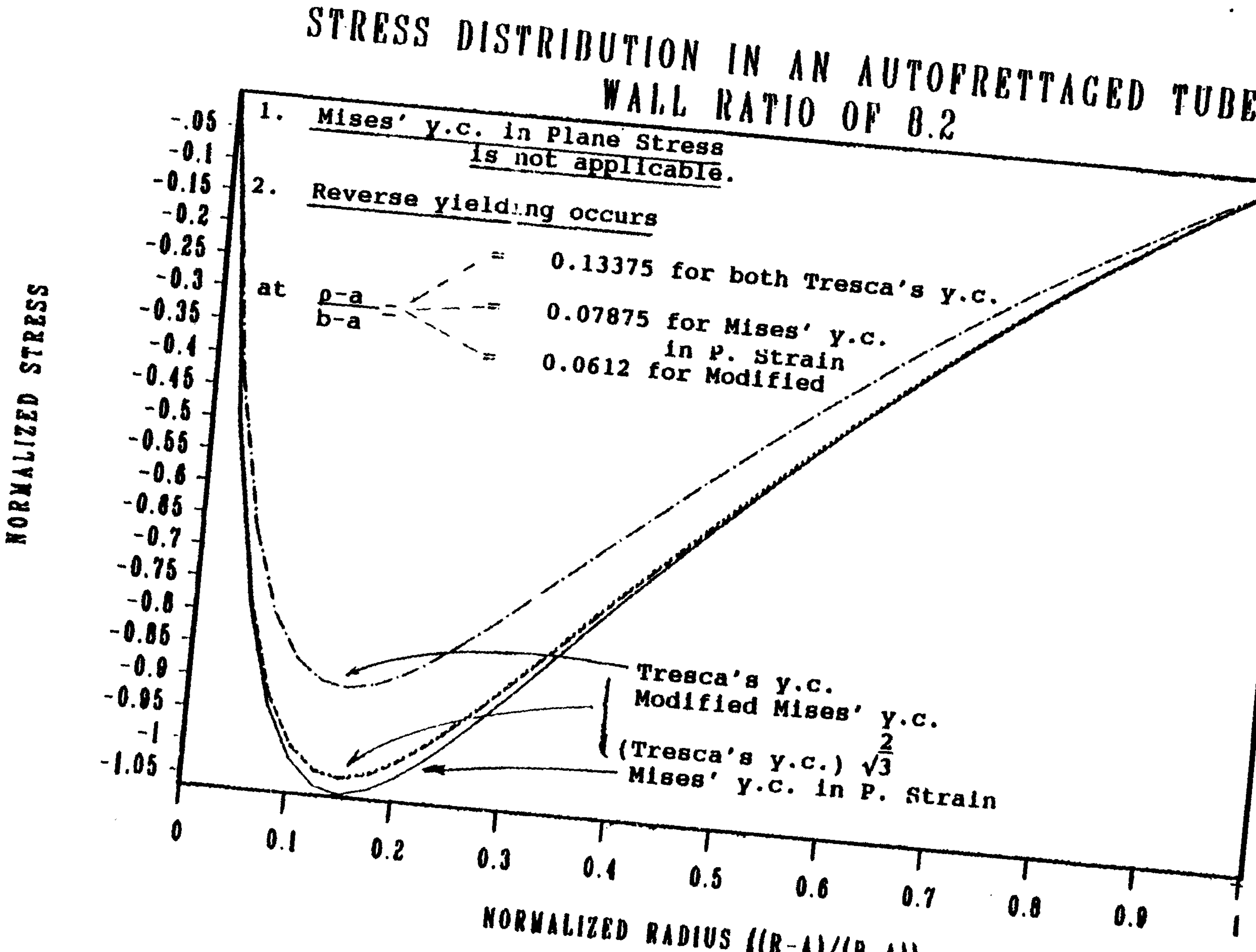

Figure 24b. **Radial stress component**: Stress distribution in an autofrettaged pressure vessel with a wall ratio of b/a = 8.2 after depressurization of 90 percent autofrettage.

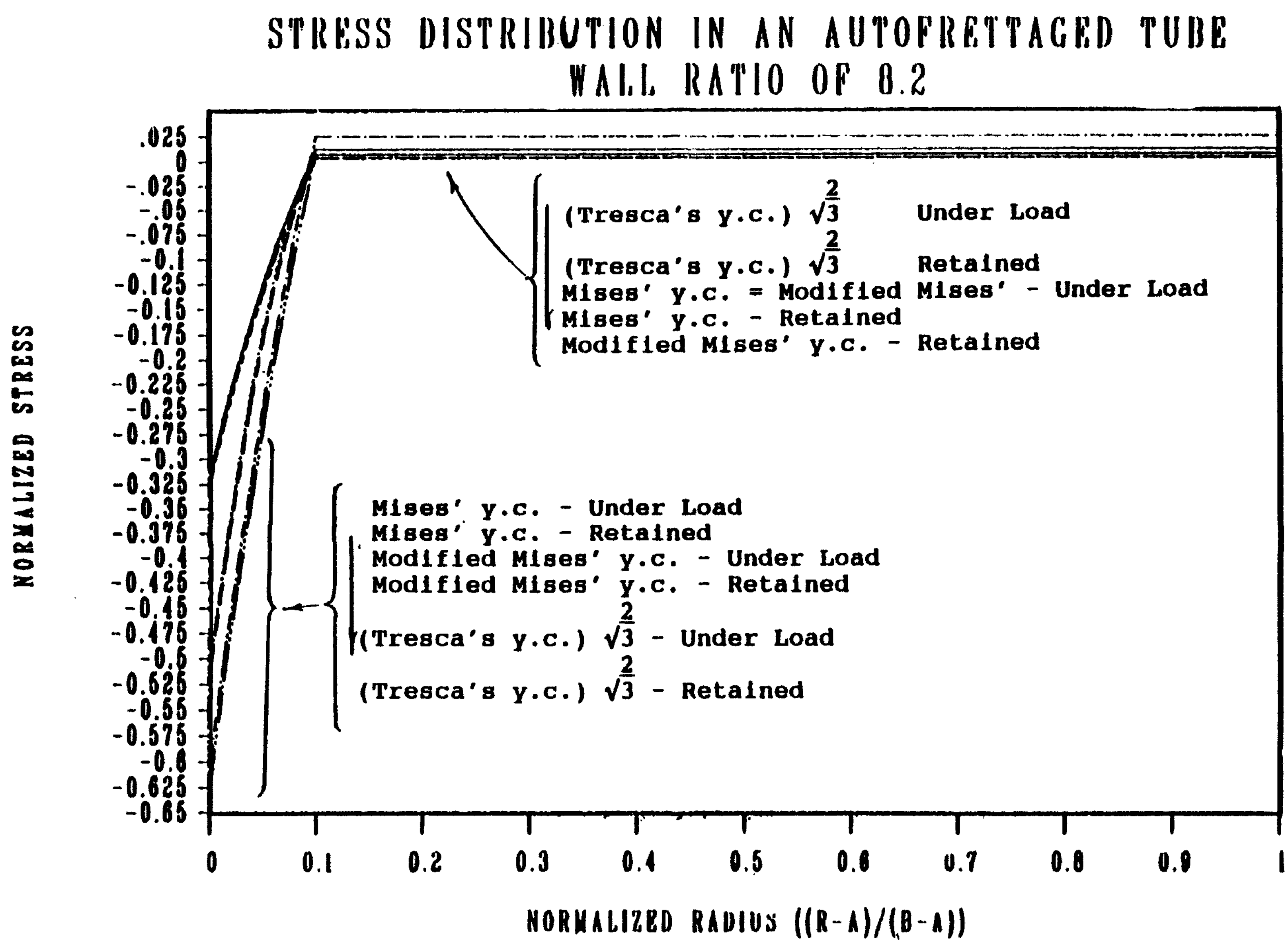

Figure 25. **Axial stress component:** Stress distribution in an autofrettaged pressure vessel with a wall ratio of b/a = 8.2 under (autofrettaging) pressure and after depressurization of 10 percent autofrettage.

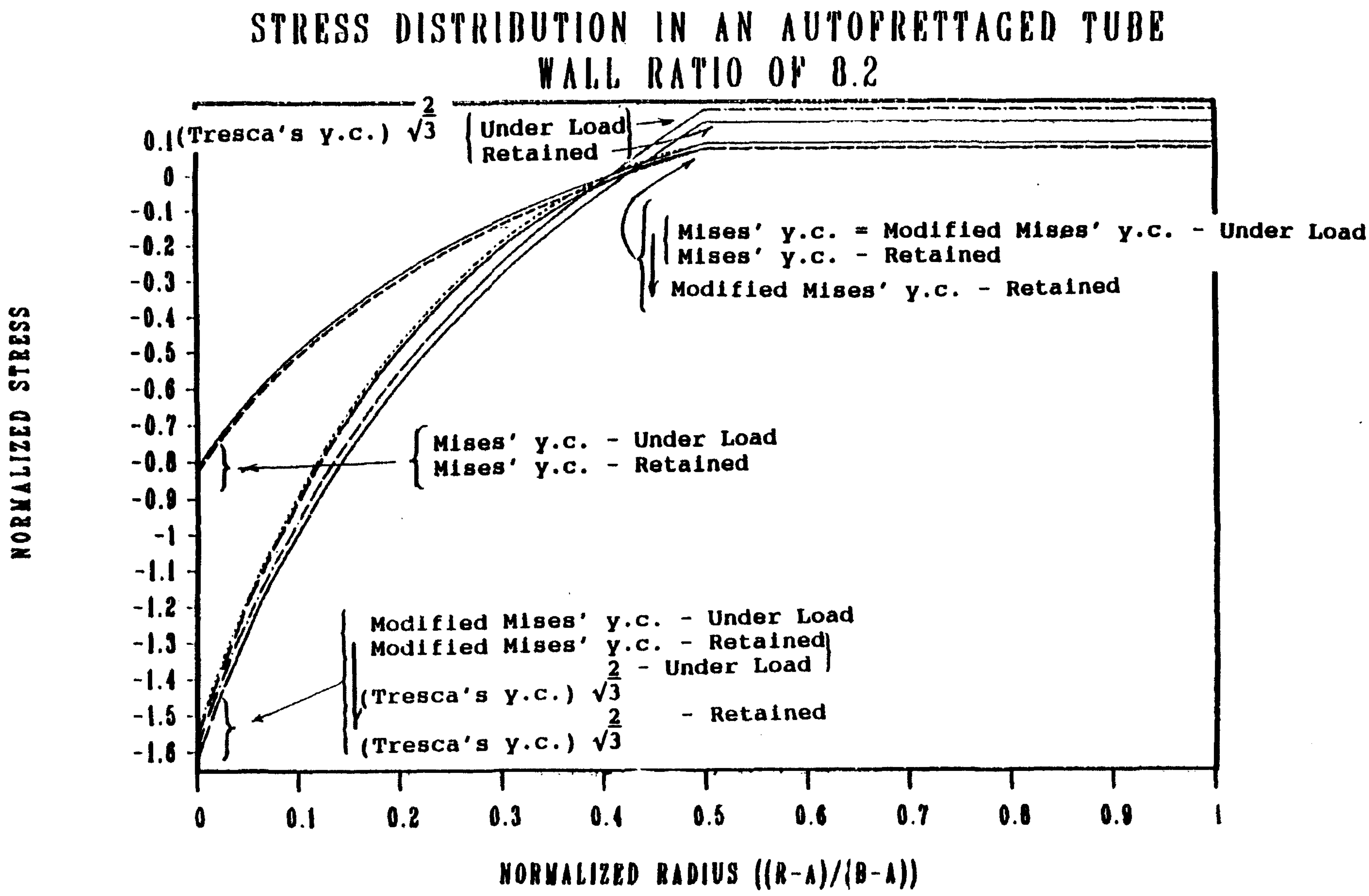

Figure 26. **Axial stress component:** Stress distribution in an autofrettaged pressure vessel with a wall ratio of b/a = 8.2 under (autofrettaging) pressure and after depressurization of 50 percent autofrettage.

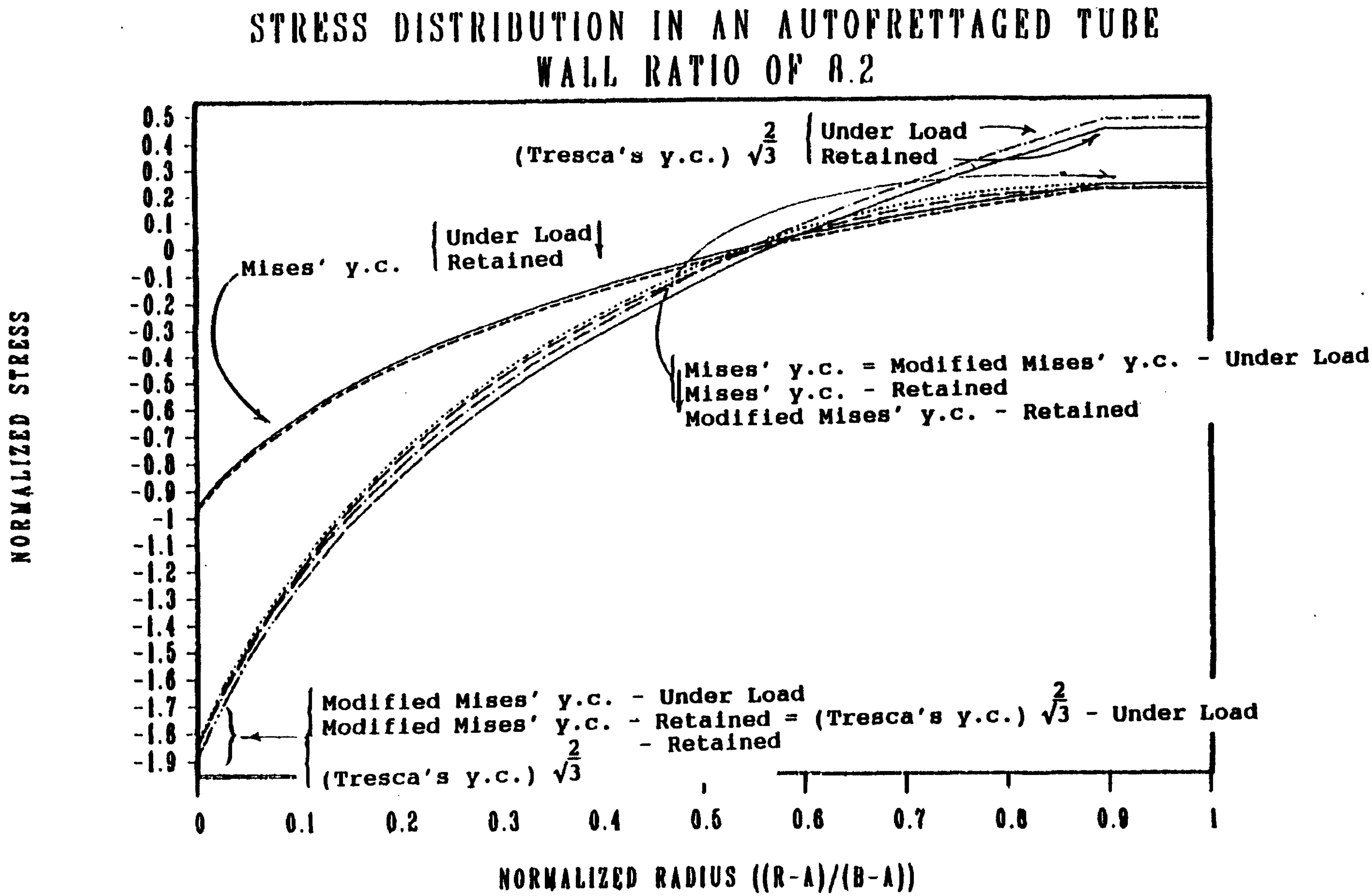

Figure 27. **Axial stress component:** Stress distribution in an autofrettaged pressure vessel with a wall ratio of b/a = 8.2 under (autofrettaging) pressure and after depressurization of 90 percent autofrettage.

TECHNICAL REPORT INTERNAL DISTRIBUTION LIST

	NO. OF COPIES
CHIEF, DEVELOPMENT ENGINEERING DIVISION	
ATTN: SMCAR-CCB-DA	1
-DC	1
-DI	1
-DR	1
-DS (SYSTEMS)	1
CHIEF, ENGINEERING SUPPORT DIVISION	
ATTN: SMCAR-CCB-S	1
-SD	1
-SE	1
CHIEF, RESEARCH DIVISION	
ATTN: SMCAR-CCB-R	2
-RA	1
-RE	1
-RM	1
-RP	1
-RT	1
TECHNICAL LIBRARY	5
ATTN: SMCAR-CCB-TL	
TECHNICAL PUBLICATIONS & EDITING SECTION	3
ATTN: SMCAR-CCB-TL	
OPERATIONS DIRECTORATE	1
ATTN: SMCWV-ODP-P	
DIRECTOR, PROCUREMENT DIRECTORATE	1
ATTN: SMCWV-PP	
DIRECTOR, PRODUCT ASSURANCE DIRECTORATE	1
ATTN: SMCWV-QA	

NOTE: PLEASE NOTIFY DIRECTOR, BENET LABORATORIES, ATTN: SMCAR-CCB-TL, OF ANY ADDRESS CHANGES.

TECHNICAL REPORT EXTERNAL DISTRIBUTION LIST

	NO. OF COPIES
ASST SEC OF THE ARMY RESEARCH AND DEVELOPMENT ATTN: DEPT FOR SCI AND TECH THE PENTAGON WASHINGTON, D.C. 20310-0103	1
ADMINISTRATOR DEFENSE TECHNICAL INFO CENTER ATTN: DTIC-FDAC CAMERON STATION ALEXANDRIA, VA 22304-6145	12
COMMANDER US ARMY ARDEC	
ATTN: SMCAR-AEE	1
SMCAR-AES, BLDG. 321	1
SMCAR-AET-O, BLDG. 351N	1
SMCAR-CC	1
SMCAR-CCP-A	1
SMCAR-FSA	1
SMCAR-FSM-E	1
SMCAR-FSS-D, BLDG. 94	1
SMCAR-IMI-I (STINFO) BLDG. 59	2
PICATINNY ARSENAL, NJ 07806-5000	
DIRECTOR US ARMY BALLISTIC RESEARCH LABORATORY ATTN: SLCBR-DD-T, BLDG. 305 ABERDEEN PROVING GROUND, MD 21005-5066	1
DIRECTOR US ARMY MATERIEL SYSTEMS ANALYSIS ACTV ATTN: AMXSY-MP ABERDEEN PROVING GROUND, MD 21005-5071	1
COMMANDER HQ, AMCCOM ATTN: AMSMC-IMP-L ROCK ISLAND, IL 61299-6000	1

	NO. OF COPIES
COMMANDER ROCK ISLAND ARSENAL ATTN: SMCRI-ENM ROCK ISLAND, IL 61299-5000	1
MIAC/CINDAS PURDUE UNIVERSITY P.O. BOX 2634 WEST LAFAYETTE, IN 47906	1
COMMANDER US ARMY TANK-AUTMV R&D COMMAND ATTN: AMSTA-DDL (TECH LIB) WARREN, MI 48397-5000	1
COMMANDER US MILITARY ACADEMY ATTN: DEPARTMENT OF MECHANICS WEST POINT, NY 10996-1792	1
US ARMY MISSILE COMMAND REDSTONE SCIENTIFIC INFO CTR ATTN: DOCUMENTS SECT, BLDG. 4484 REDSTONE ARSENAL, AL 35898-5241	2
COMMANDER US ARMY FGN SCIENCE AND TECH CTR ATTN: DRXST-SD 220 7TH STREET, N.E. CHARLOTTESVILLE, VA 22901	1
COMMANDER US ARMY LABCOM MATERIALS TECHNOLOGY LAB ATTN: SLCMT-IML (TECH LIB) WATERTOWN, MA 02172-0001	2

NOTE: PLEASE NOTIFY COMMANDER, ARMAMENT RESEARCH, DEVELOPMENT, AND ENGINEERING CENTER, US ARMY AMCCOM, ATTN: BENET LABORATORIES, SMCAR-CCB-TL, WATERVLIET, NY 12189-4050, OF ANY ADDRESS CHANGES.

TECHNICAL REPORT EXTERNAL DISTRIBUTION LIST (CONT'D)

	NO. OF COPIES
COMMANDER US ARMY LABCOM, ISA ATTN: SLCIS-IM-TL 2800 POWDER MILL ROAD ADELPHI, MD 20783-1145	1
COMMANDER US ARMY RESEARCH OFFICE ATTN: CHIEF, IPO P.O. BOX 12211 RESEARCH TRIANGLE PARK, NC 27709-2211	1
DIRECTOR US NAVAL RESEARCH LAB ATTN: MATERIALS SCI & TECH DIVISION CODE 26-27 (DOC LIB) WASHINGTON, D.C. 20375	1 1
COMMANDER AIR FORCE ARMAMENT LABORATORY ATTN: AFATL/MN EGLIN AFB, FL 32542-5434	1
COMMANDER AIR FORCE ARMAMENT LABORATORY ATTN: AFATL/MNF EGLIN AFB, FL 32542-5434	1
DIRECTOR US ARMY BALLISTIC RESEARCH LABORATORY ATTN: SLCBR-IB-M (DR. BRUCE BURNS) ABERDEEN PROVING GROUND, MD 21005-5066	1

NOTE: PLEASE NOTIFY COMMANDER, ARMAMENT RESEARCH, DEVELOPMENT, AND ENGINEERING CENTER, US ARMY AMCCOM, ATTN: BENET LABORATORIES, SMCAR-CCB-TL, WATERVLIET, NY 12189-4050, OF ANY ADDRESS CHANGES.